IMPROVED MODELING OF PSEUDO PSEUDO-STEADY STATE FLOW REGIME IN UNCONVENTIONAL RESERVOIR

A Thesis

by

HANYU LI

Submitted to the Office of Graduate and Professional Studies of
Texas A&M University
in partial fulfillment of the requirements for the degree of

MASTER OF SCIENCE

Chair of Committee,	Michael King
Committee Members,	Ahkil Datta-Gupta
	Thomas Blasingame
Head of Department,	Dan Hill

May 2017

Major Subject: Petroleum Engineering

ABSTRACT

Unconventional resources which are generally categorized by their extremely low permeability and high heterogeneity have become increasingly appealing over recent years. The typical development strategy is drilling horizontal wells with tight spacing hydraulic fractures. Such strategy leads to a significant loss of flowing area during fracture interference, thus resulting in a transition flow regime with unit slope identified as pseudo pseudo-steady state flow. Capturing such flow regime is critical in delivering accurate reservoir performance analysis. This thesis discusses a methodology to accurately capture drainage and pressure depletion behavior of horizontal wells with multiple hydraulic fractures. We will use asymptotic solution with separation of variables in order to model the pseudo pseudo-steady state flow regime. A more precise modeling of pressure behavior with analytical asymptotic solution ensures more confident reservoir forecast with low computation time.

Traditionally, we utilize two main methods to conduct unconventional reservoir calibration and forecast in order to obtain Estimated Ultimate Recovery (EUR). The first one is an analytical method such as decline curve analysis. It is a simplified empirical method which is time efficient however also ignores vital information such as complex geometries. The second method is by numerical simulation which takes into account of the geometries and heterogeneity, but is also time consuming especially when reservoir models contain millions of grid cells.

The Fast Marching Method emerges as a novel approach to calibrate and forecast reservoir performance with significantly reduced calculation time. The validity of this method has been tested in transient phase (infinite acting flow regime) of pressure diffusion. However, considering the vast existence of hydraulic fractured horizontal wells in unconventional reservoirs, adjacent fractures create virtual boundary conditions. Accordingly, the flow regime associated with hydraulic fractured horizontal wells is channel flow. Such flow regime is characterized by pressure front encountering boundary conditions in one direction while remain infinite acting in the perpendicular direction. Therefore we introduce the separation of variables in order to analyze pressure front propagation in these two directions independently. Such method optimizes the calculation of drainage volume in channel flow scenario, thus capable of modeling the signature feature of unconventional reservoirs, pseudo pseudo-steady state flow regime, more accurately. The results from this methodology is compared against the ones from numerical simulation as validation.

DEDICATION

The dedication of this thesis is split in three ways.

To my beloved parents for their selfless support.

To my advisor and committee members for their precious guidance.

And to my friends who shared my happiness and sorrow.

ACKNOWLEDGEMENTS

First, I would like to thank my committee chair, Dr. Michael King for being an amazing advisor and embark me on this research journey since my junior year during my undergraduate study.

I would also like to extend my gratitude to my other committee members, Dr. Akhil Datta-Gupta and Dr. Thomas Blasingame for their support during the course of this research.

Thanks also go to my friends and colleagues and the department faculty and staff for making my time at Texas A&M University a great experience.

Finally, thanks to my mother and father for their encouragement and help me through many hard times of my life.

CONTRIBUTORS AND FUNDING SOURCES

Contributors

Part 1, faculty committee recognition

This work was supervised by a thesis (or) dissertation committee consisting of Professor Michael King and Professor Ahkil Datta-Gupta of the Department of Petroleum Engineering and Professor Thomas Blasingame of the Department of Geophysics.

Part 2, student/collaborator contributions

All work for the thesis (or) dissertation was completed independently by the student.

Funding Sources

Graduate study was supported by a fellowship from Texas A&M University and a graduate research assistantship from CMG Foundation.

NOMENCLATURE

c_t	Total compressibility
k	Permeability
p	Pressure
p_{wf}	Bottom hole flowing pressure
q	Flux
q_w	Flux at surface
r	Distance
R	Reflection coefficient
t	Time
T	Transmission coefficient
$V(t)$	Time dependent volume
$V_d(t)$	Drainage Volume
$V_p(\tau)$	Pore volume
$w(\tau)$	Derivative of pore volume with respect to τ
$w_{left}(\tau)$	$w(\tau)$ on the left domain at the boundary condition
$w_{right}(\tau)$	$w(\tau)$ on the right domain at the boundary condition

Greek variables

α	Hydraulic diffusivity
μ	Viscosity
τ	Diffusive time of flight
τ_d	Diffusive time of flight at boundary
ϕ	Porosity

Abbreviations

IARF	Infinite Acting Radial Flow
BDF	Boundary Dominated Flow
PSS	Pseudo-steady State Flow
PPSS	Pseudo Pseudo-steady State Flow
FMM	Fast Marching Method
EUR	Estimated Ultimate Recovery
DTOF	Diffusive Time of Flight
DCA	Decline Curve Analysis
PTA	Pressure Transient Analysis
RTA	Rate Transient Analysis

TABLE OF CONTENTS

Page

LIST OF FIGURES

Page

LIST OF TABLES

Page

CHAPTER I

INTRODUCTION AND LITERATURE REVIEW

1.1 US Unconventional Resources Overview

Several significant unconventional reservoirs in the United States shown Fig.1 has been discovered in the past 20 years. With the recent technology advancement in horizontal drilling and hydraulic fracturing, we have observed a dramatic production increase from the shale plays since 2006 as illustrated in Fig.2.

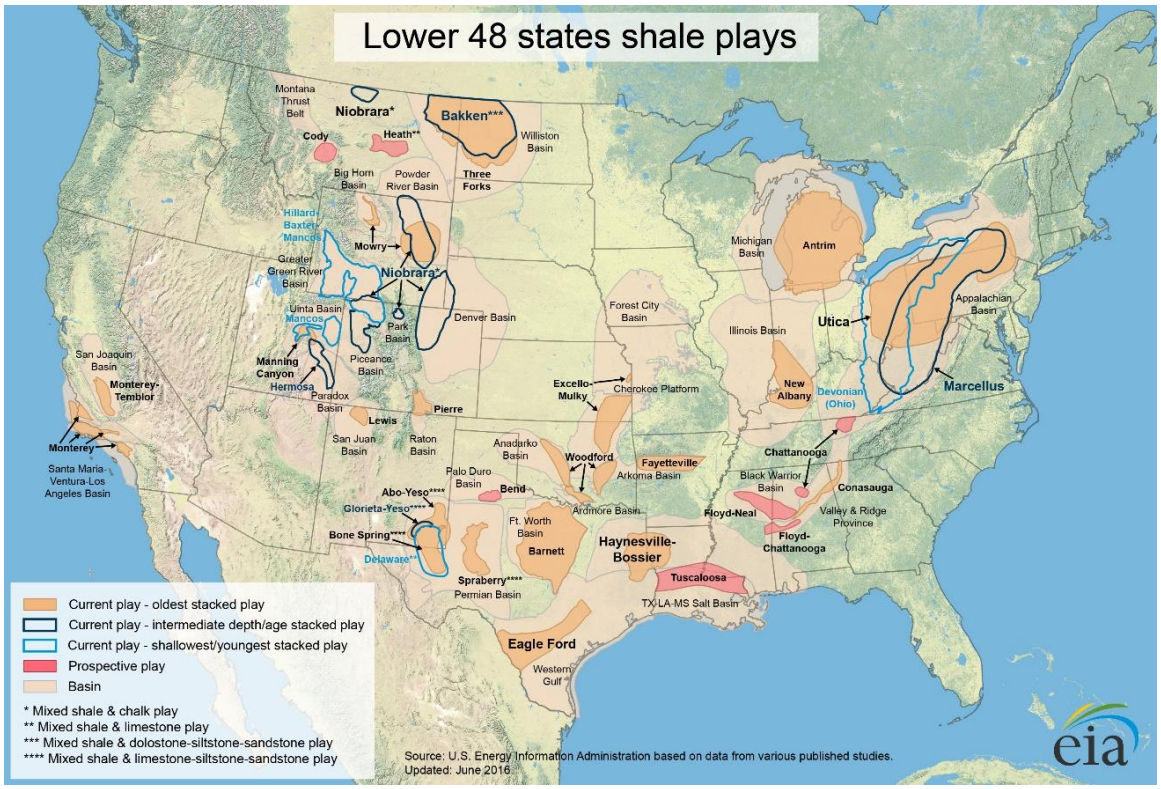

Fig.1 U.S. Major Shale Plays Map, U.S EIA Maps, Reprinted from https://www.eia.gov/maps/images/shale_gas_lower48.pdf

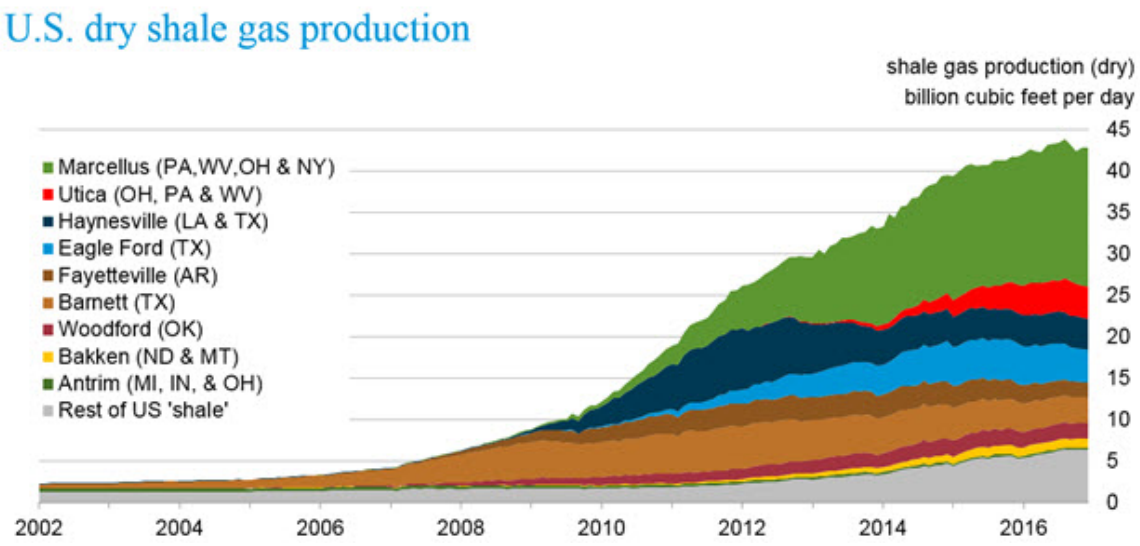

Fig.2 U.S. Dry Shale Gas Production from Major Shale Plays, U.S. EIA, Reprinted from https://www.eia.gov/energyexplained/index.cfm?page=natural_gas_where

U.S. Energy Information Administration projected in Fig.3 that shale gas will contribute to almost 40% of U.S. dry natural gas production by 2040.

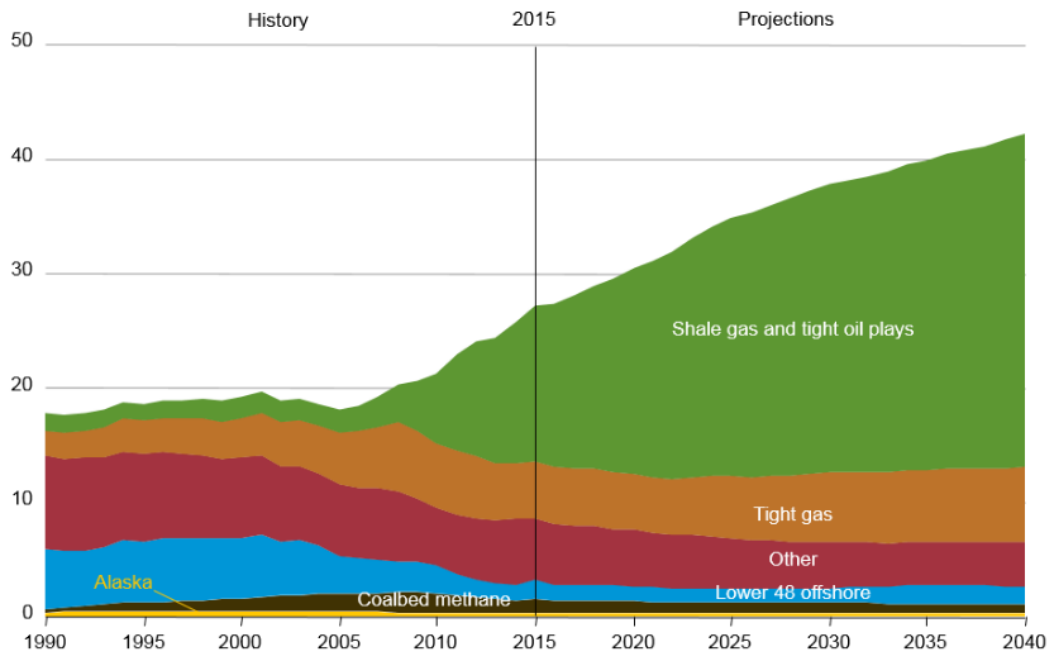

Fig.3 U.S. Dry Gas Production History and Projection in Tcf/Year (Reprinted from EIA Annual Energy Outlook 2016)

With the massive volume of shale reserves and continuous development, this so-called shale boom tends to transform U.S. into an energy self-sustaining country in the near future. Under such atmosphere, in order to develop unconventional reservoirs more efficiently, the demand for technology capable of optimizing development strategy and minimize expenditure is urgent. To achieve such goal, engineers confront a number of challenges to comprehensively understand the natural mechanisms in unconventional reservoirs, including the fluid flow behavior after the pore scale falls into the Nano range.

The industry has adopted several methods to analyze shale plays. The type curve for decline curve analysis (Fetkovich 1980) was first created to analyze conventional

reservoir ultimate recovery. This approach mainly involves curve-fitting the production history and extrapolate the fitted curve for production forecast and obtain Estimated Ultimate Recovery. The Fetkovich type curve is valid for vertical wells producing under boundary dominated flow regime which is widely observed in conventional reservoirs. However for unconventional reservoirs, considering the extremely low permeability, the economic production is usually carried by hydraulic fractured horizontal wells. Also because of the low permeability, the transient flow lasts a very long time (typically years) and it is almost impossible to achieve boundary dominated flow. In response to the above situations denying the applicability of Fetkovich analysis, type curves to analyze unconventional reservoirs are created (Valko el al. 2010). This novel approach introduced the Stretched Exponential Production Decline model which captures the finite behavior of EUR for unconventional wells.

The pressure and rate transient analysis (PTA & RTA) are also powerful tools to analyze the reservoir. The PTA uses early time data to quantify reservoir properties such as permeability and estimate the distance to boundaries (Lee 1982). The RTA uses the boundary dominated flow data to estimate ultimate recovery. However, at sufficiently low permeability, the time required for the pressure diffusion to travel a certain distance increases dramatically as shown in Fig.4.

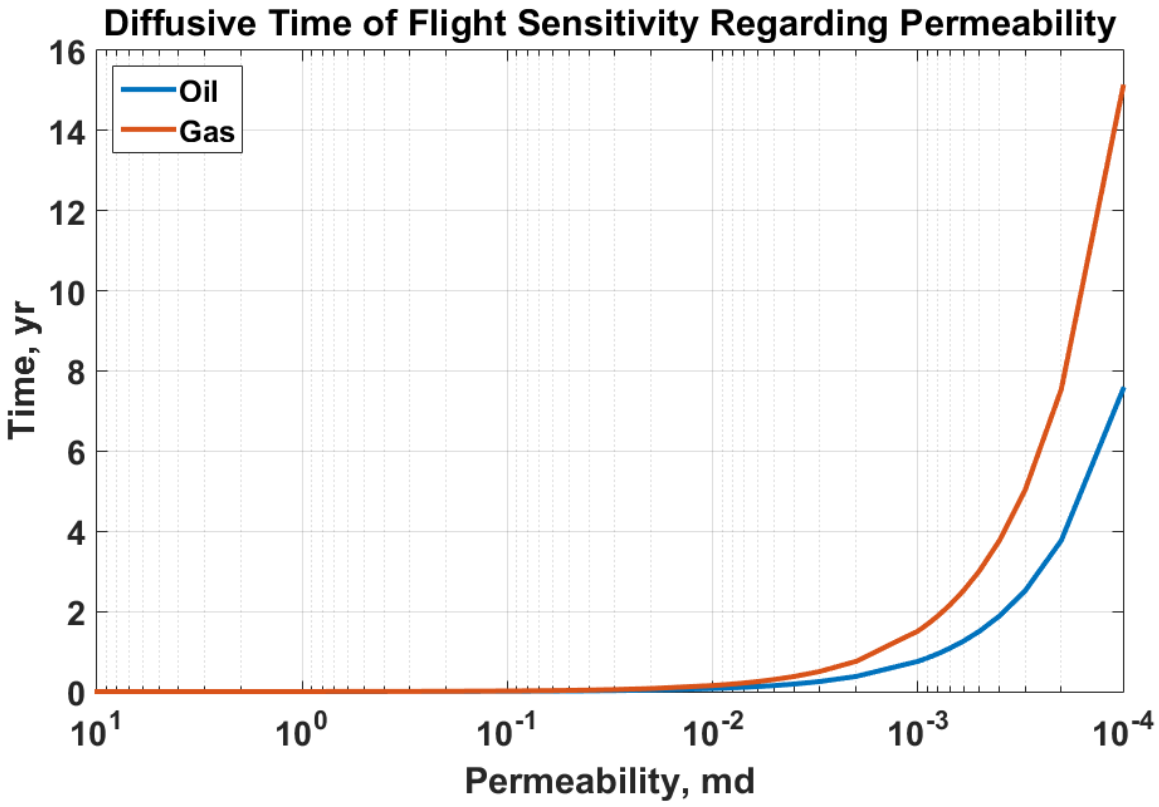

Fig.4 Time Required for Pressure Diffusion to Travel 220 Feet Regarding Different Permeability

Under such circumstances, the required flow regime for RTA is hardly achievable and the clear distinction between PTA and RTA vanishes. Correspondingly, we use rate-normalized pressure analysis to forecast well performance (Bo Song et al. 2011).

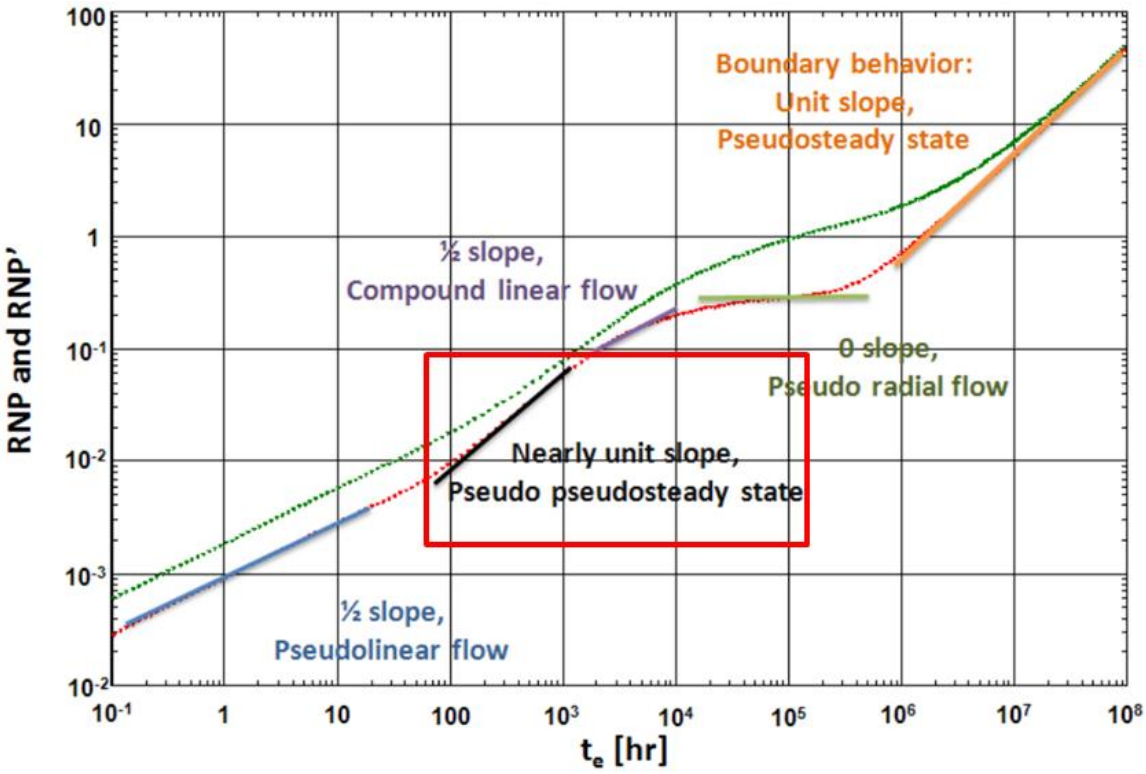

Fig.5 Pseudo Pseudo-steady state Following Initial Fracture Linear Flow (Reprinted from Song et al. 2011)

Bo Song identified pseudo pseudo-steady state flow regime in his paper (Fig.5) and emphasized that capturing such flow regime is essential for delivering accurate reservoir forecast such as EUR in unconventional plays.

Pseudo pseudo-steady state flow usually appears in unconventional reservoirs where the typical development strategy is long fracture and tight spacing. Such fracture geometry defines the Stimulated Reservoir Volume (SRV) illustrated in Fig.6.

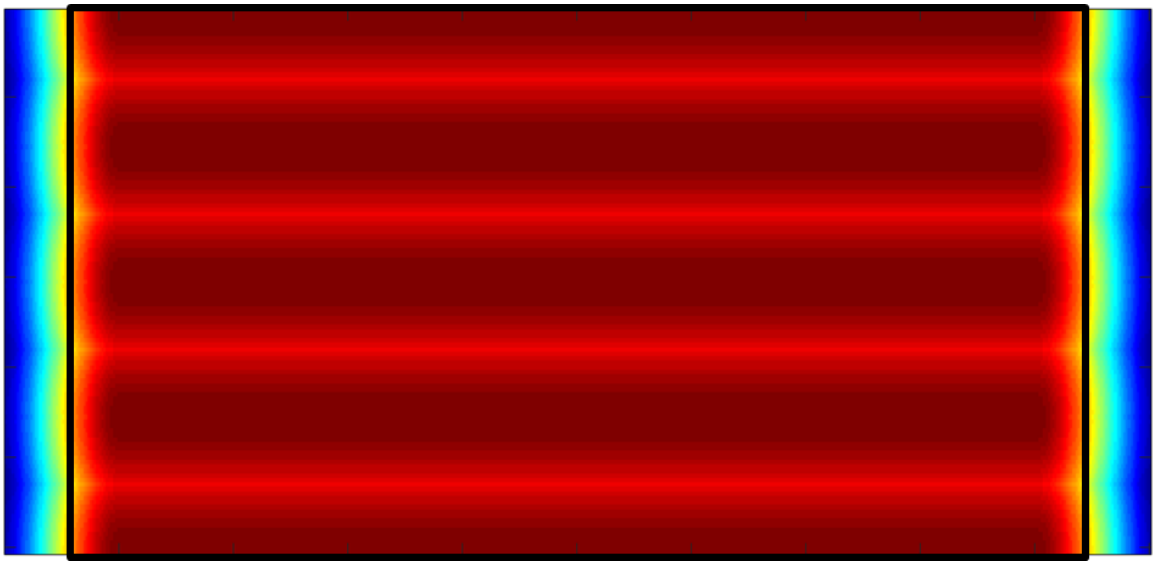

Fig.6 Fracture Geometry Defines Drainage Volume

When the drainage from SRV is completed, the well experiences a significant loss of flowing area. Accordingly, the diagnostic plot undergoes a sharp transition period with a nearly positive unit slope. Thus we observe pseudo pseudo-steady state flow.

1.2 Asymptotic Solution

Both decline curve analysis and pressure/rate transient analysis are analytical solutions which provides result with competitive calculation time. However, neither of them takes into account of complex geometries, heterogeneity and natural phenomenon such as fracture closure. Therefore, in the interest of improving the accuracy of reservoir forecast, the industry also adopted numerical simulation to model the complicated reservoir mechanisms (Cipolla et al. 2009, Cullick et al. 2014). Not only does it rigorously captures natural behaviors such as fracture closure (Friedrich et al. 2013),

numerical simulation also incorporates a large variety of data such as microseismics and well log (Dinh et al. 2015), and thus providing more reliable EUR. However the related calculation time increases dramatically, especially for reservoir models with millions of grid cells.

In order to decrease calculation time while maintaining the forecast accuracy by considering factors such as complex geometries, the industry seeks to evolve a new approach from pressure transient analysis. According to the diffusivity equation which governs the pressure behavior in porous media, the characteristics of pressure diffusion such as diffusive time of flight, radius of investigation and front shape, are controlled by the reservoir and fluid properties such as permeability heterogeneity and viscosity. Modeling the pressure or rate normalized pressure behavior with the production data indicates a successful calibration.

The diffusivity equation is a non-linear partial differential equation extremely difficult to solve analytically in real domain. Therefore, to obtain a simpler version of diffusivity equation, we apply the concept from diffusive electromagnetic imaging (Virieux et al. 1994) to describe the pressure diffusion in frequency domain. The solution to the frequency domain diffusivity equation give rise to the asymptotic solution which describe the pressure diffusion in porous media as a propagating front. Such propagating front refers to the maximum pressure disturbance created by a source or sink (Vasco et al. 2000, Kulkarni et al. 2001, Datta-Gupta et al. 2007).

In electromagnetic wave propagation, when the wave reaches the interface of two medium, part of it is reflected into the same medium while the remaining part is

transmitted to the other medium (Jackson, 1998). The asymptotic solution which relies on the analogy between pressure diffusion and electromagnetic wave propagation allows us to apply the reflection and transmission mechanism into pressure diffusion. Such application is useful to model pressure behavior in composite reservoirs and boundary conditions (King et al. 2016). The composite reservoir situation usually arises when there is thick skin region near the wellbore that causes a sudden change in hydraulic diffusivity (Satman et al. 1980, Gringarten et al. 2000, Muskat 1949, Hawkins 1956). What's more exciting is its ability to model the boundary conditions, present as either actual boundaries at formation intersect or virtual boundaries created by pressure interference such as adjacent fracture interference. Capturing pressure and drainage behavior during fracture interference allows us to capture signature flow regime of unconventional reservoirs.

The high frequency limit solution to frequency domain diffusivity equation gives rise to the Eikonal equation. The Eikonal equation can be solved very efficiently by the Fast Marching Method (Sethian 1996) for the diffusive time of flight. This methodology is a vital tool for us to apply the reflection and transmission mechanism into heterogeneous cases.

1.3 Fast Marching Method

Regarding to DCA, PTA and RTA, all of them rely on assumptions of homogeneous reservoir and simple geometry. The Fast Marching Method emerges as a novel methodology that is capable of including vital information such as heterogeneity

and complex geometry (Xie et al. 2015a, 2015b). While this approach simulates pressure diffusion instead of actually solving the flow mechanism, its required computation time is very competitive. The FMM solves the Eikonal equation non-iteratively to provide the pressure propagating front. Such calculation only requires seconds to complete for a model with several millions of cells. The DTOF provided by FMM is useful for asymptotic solution to calculate the drainage volume and well test derivative. The combination of these two methods provides us a powerful tool to analyze highly heterogeneous unconventional reservoirs.

1.4 Outline of the Thesis

In this thesis, we already provided a brief history of unconventional reservoir analysis and the method we have been developing. In the next chapter, we will first introduce the detailed concept and mathematic derivation of asymptotic solution and separation of variables which we use to improve the modeling of pseudo pseudo-steady state flow regime. Following the derivation, we will use vertical wells flowing at constant rate in homogeneous reservoir to test the validity of separation of variables. In Chapter III, we will use such methodology to investigate several fracture cases. We will start with single fracture to investigate possible problems our method has when analyzing fractures. Then we will test multiple fractures with tight spacing in homogeneous reservoir. Such scenario will confirm whether we will be able to model PPSS flow regime with our methodology. We will apply both constant flow rate and constant bottom hole flowing pressure. After homogeneous reservoir analysis as a

thorough validation of our approach, we will extend our methodology into heterogeneous reservoirs in Chapter IV. To do so, we will need to solve several problems. First is to determine irregular stagnation line caused by fracture interference in the presence of heterogeneity and correctly decompose the total DTOF into two directions. Secondly, we need to find the most appropriate way to determine the boundary diffusive time of flight as the reflection indicator. With these problems solved, we will once again try to model PPSS flow regime in heterogeneous media. After showing the results, we will draw conclusions and recommendations in Chapter V.

CHAPTER II

METHODOLOGY OF APPLYING SEPARATION OF VARIABLES TO ASYMPTOTIC SOLUTION

In this chapter, we will first describe the concept of radius of investigation and diffusivity equation as the background knowledge. These two concepts are mainly applicable in homogeneous reservoirs. In order to solve diffusivity equation and calculate drainage volume in heterogeneous cases, the asymptotic solution is derived using the analogy between pressure diffusion and wave propagation. Afterwards, we will introduce the separation of variables method which benefits the calculation of drainage volume under linear follow regime. Linear flow is generally observed in multistage fractured horizontal wells producing in unconventional reservoir. By using this methodology, we hope to model PPSS flow regime and achieve higher accuracy when conducting unconventional reservoir analysis.

2.1 Diffusivity Equation and Radius of Investigation

The diffusivity equation governs the pressure diffusion behavior in the reservoir. It is created by combining three equations. The first equation called continuity equation which describes the conservation of mass.

$$\nabla \cdot (\rho v) = -\frac{\partial}{\partial t}(\rho \phi) \tag{2.1}$$

The second equation is the well-known Darcy's Law which describes the fluid movement through the porous media under the influence of pressure gradient.

$$v = -\frac{k}{\mu}(\Delta p) \tag{2.2}$$

And the equation of states describes the fraction change of volume under pressure

$$c = \frac{1}{\rho}\left(\frac{d\rho}{dp}\right) \tag{2.3}$$

By combining Eq.(2.1) (2.2) (2.3), we obtain the diffusivity equation in homogeneous reservoir as

$$\frac{\phi\mu c_t}{k}\frac{\partial p}{\partial t} = \nabla^2 p \tag{2.4}$$

Rewritten Eq.(2.4) in radial coordinates we have

$$\frac{\phi\mu c_t}{k}\frac{\partial p}{\partial t} = \frac{1}{r}\frac{\partial}{\partial r}\left(r\frac{\partial p}{\partial r}\right) \tag{2.5}$$

We can solve the diffusivity equation in homogeneous reservoir analytically using either Boltzmann transform or Laplace transform.

When a well produces from an undisturbed reservoir or is shut in from a period of production, it creates pressure disturbance which propagates from the well into the reservoir. Such pressure disturbance behavior can be described by Eq.(2.5). Consider a well with negligible wellbore radius producing at a constant rate in a homogeneous reservoir, the pressure disturbance will diffuse in complete circles. The radius of such circle which indicates how far the pressure disturbance has propagated is known as the Radius of Investigation (Lee 1982). Dr. Lee defined the radius of investigation as the

location with the maximum value of pressure disturbance ($\frac{\partial \Delta p}{\partial t}$) and is calculated in radial flow regime as

$$r = \sqrt{\frac{kt}{948\phi\mu c_t}} \tag{2.6}$$

The radius of investigation is considered as the footprint of the drainage volume from a well. Indicated by Eq.(2.6), such drainage volume is only affected by reservoir and fluid properties but not flow rate.

2.2 Derivation of Asymptotic Solution from Diffusivity Equation

When encountering heterogeneous reservoirs, we can no longer solve the diffusivity equation analytically with Boltzmann transform or Laplace transform. Therefore we introduce the asymptotic solution. By rewriting Eq.(2.4) in heterogeneous cases with porosity and permeability varying at different location we have

$$\phi\left(\vec{x}\right)\mu c_t \frac{\partial p\left(\vec{x},t\right)}{\partial t} = \nabla \cdot \left[k\left(\vec{x}\right) \cdot \nabla p\left(\vec{x},t\right) \right] \tag{2.7}$$

After applying Fourier transform, we can obtain diffusivity equation in frequency domain as

$$\phi\left(\vec{x}\right)\mu c_t \left(-i\omega\right) p\left(\vec{x},\omega\right) - \nabla \cdot \left[k\left(\vec{x}\right) \cdot \nabla p\left(\vec{x},\omega\right) \right] = 0 \tag{2.8}$$

The solution to diffusivity equation in frequency domain draws upon the analogy between pressure diffusion and electromagnetic wave propagation. Therefore by

utilizing the concepts from diffusive electromagnetic imaging (Virieux et al. 1994), we can obtain the solution in frequency domain as

$$p\left(\vec{x},\omega\right)=e^{-\sqrt{-i\omega\tau}\left(\vec{x}\right)}\sum_{k=0}^{\infty}\frac{A_k\left(\vec{x}\right)}{\left(\sqrt{-i\omega}\right)^k} \tag{2.9}$$

The high frequency limit ($\omega\to\infty$) solution of Eq.(2.9) gives rise to the Eikonal equation.

$$\nabla\tau\left(\vec{x}\right)\cdot\bar{\bar{k}}\left(\vec{x}\right)\cdot\nabla\tau\left(\vec{x}\right)=\phi\left(\vec{x}\right)\mu c_t \tag{2.10}$$

The term τ is known as the diffusive time of flight (DTOF). For homogeneous cases, the diffusive time of flight can be expressed as

$$\tau=\sqrt{\frac{\phi\mu c_t}{k}}r \tag{2.11}$$

In heterogeneous cases, considering the permeability and porosity varies at different location, we usually express the incremental diffusive time of flight as

$$d\tau=\sqrt{\frac{\phi\left(\vec{x}\right)\mu c_t}{k\left(\vec{x}\right)}}dr \tag{2.12}$$

The Fast Marching Method first introduced by Sethian (1996) is capable of solving the Eikonal equation very efficiently. It is applied to calculate diffusive time of flight for heterogeneous media. An example FMM is illustrated in Fig.7.

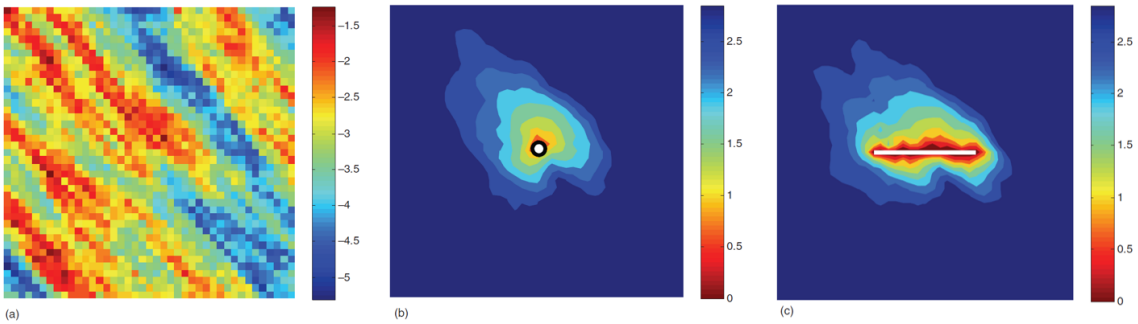

Fig.7 Solution of Diffusivity Equation in Heterogeneous Medium Using Fast Marching Method (a) Log Permeability Field (b) Pressure Contour for a Vertical Well (c) for a Vertical Well with an Infinite Conductivity Fracture (Reprinted from Datta-Gupta, et. al 2011)

Assuming that pressure contour overlaps the DTOF contour, we can perceive the reservoir as acting in pseudo-steady state flow within each τ contour, enabling us to integrate the 3-D diffusivity equation into the equivalent 1-D diffusivity equation. Let us start with the material balance equation relating average reservoir pressure with flux (Matthews et al. 1954).

$$c_t V_p(\tau)\frac{\partial p(\tau,t)}{\partial t} = -q_w + q(\tau,t) \tag{2.13}$$

Eq.(2.13) describes the average reservoir pressure up to a certain DTOF contour. Instead, if we only calculate the pressure within a very thin volume between two τ contours, Eq.(2.13) becomes

$$c_t \frac{\partial p(\tau,t)}{\partial t} = \frac{\partial q(\tau,t)}{\partial V_p(\tau)} = \frac{1}{w(\tau)}\frac{\partial q(\tau,t)}{\partial \tau} \tag{2.14}$$

The $w(\tau)$ term represents the thin volume between two discretized DTOF contour and is expressed as

$$w(\tau) = \frac{dV_p(\tau)}{d\tau} \tag{2.15}$$

We can relate flux with pressure by Darcy's Law in DTOF coordinates by

$$q = c_t w(\tau) \frac{\partial p}{\partial \tau} \tag{2.16}$$

Substituting Eq.(2.16) into Eq.(2.14) gives rise to the equivalent 1-D diffusivity equation

$$\frac{\partial p(\tau,t)}{\partial t} = \frac{1}{w(\tau)} \frac{\partial}{\partial \tau}\left(w(\tau) \frac{\partial p(\tau,t)}{\partial \tau} \right) \tag{2.17}$$

We can also rewrite the 1-D diffusivity equation in flux form by inverting the $w(\tau)$ term

$$\frac{\partial q(\tau,t)}{\partial t} = w(\tau) \frac{\partial}{\partial \tau}\left(\frac{1}{w(\tau)} \frac{\partial q(\tau,t)}{\partial \tau} \right) \tag{2.18}$$

With the altered diffusivity equation, we can model pressure diffusion propagating out in τ contour in heterogeneous media shown in Fig.8.

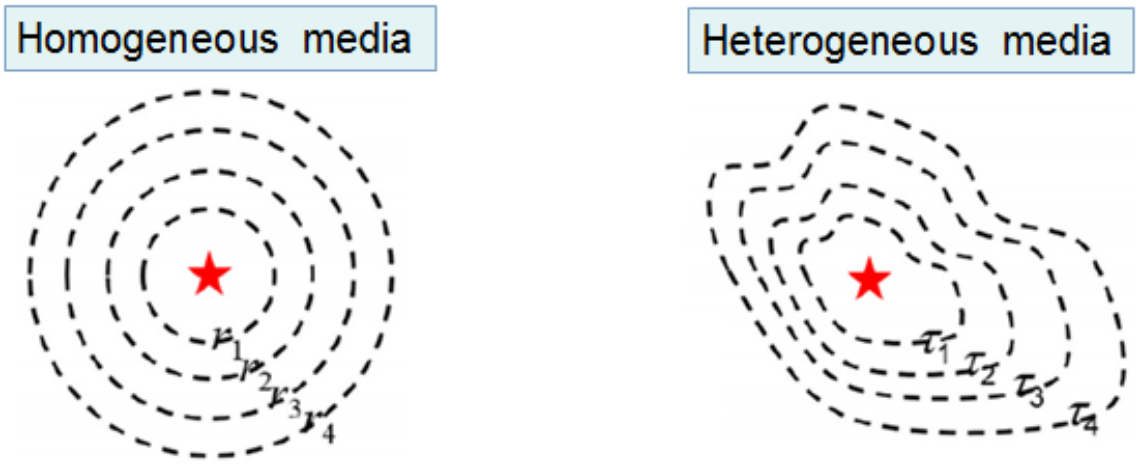

Fig.8 Pressure Diffusion in both Homogeneous Media and Heterogeneous Media (Reprinted from Yang et al. 2015)

The flux is dependent upon location and time. In 1-D τ coordinate system we denoted as $q(\tau,t)$. Assuming self-similarity, by using the Boltzmann variable, which relates t and τ as $\xi=\frac{\tau^2}{4t}$, we can relate the change of flux respect to time to change of flux respect to DTOF.

$$\frac{\partial q}{\partial \tau}=\frac{\partial q}{\partial \xi}\frac{\partial \xi}{\partial \tau}=\frac{\partial q}{\partial \xi}\frac{\tau}{2t} \tag{2.19}$$

$$\frac{\partial q}{\partial t}=\frac{\partial q}{\partial \xi}\frac{\partial \xi}{\partial t}=\frac{\partial q}{\partial \xi}\left(-\frac{\tau^2}{4t^2}\right) \tag{2.20}$$

$$\frac{\partial q}{\partial t}=\left(-\frac{\tau}{2t}\right)\frac{\partial q}{\partial \tau} \tag{2.21}$$

Substituting Eq.(2.21) into Eq.(2.18) yields

$$\left(\frac{1}{w(\tau)}\frac{\partial q(\tau,t)}{\partial \tau}\right)^{-1}\frac{\partial}{\partial \tau}\left(\frac{1}{w(\tau)}\frac{\partial q(\tau,t)}{\partial \tau}\right)=\frac{\partial}{\partial \tau}\left[\ln\left(\frac{1}{w(\tau)}\frac{\partial q(\tau,t)}{\partial \tau}\right)\right]=-\frac{\tau}{2t} \tag{2.22}$$

We observe that if we integrate Eq.(2.22), the term $\left(\frac{1}{w(\tau)}\frac{\partial q(\tau,t)}{\partial \tau}\right)$ follows an exponential decay. If this behavior is incorporated into the mass balance equation, Eq.(2.14) becomes

$$c_t \frac{\partial p(\tau,t)}{\partial t} = \frac{1}{w(\tau)}\frac{\partial q(\tau,t)}{\partial \tau} \approx -\frac{q_w}{V(t)} e^{-\frac{\tau^2}{4t}} \tag{2.23}$$

The term $\frac{\partial q(\tau,t)}{\partial V_p(\tau)}$ is denoted as the flow rate and drainage volume at the well ($\tau = 0$) scaled by the exponential factor. The drainage volume is calculated by integrating the thin volume between DTOF contours at a specific time.

$$V(t) = \int_0^\infty w(\tau) \cdot e^{-\frac{\tau^2}{4t}} \cdot d\tau \tag{2.24}$$

In the formulation, only the part of reservoir acting in pseudo-steady state and transition flow regime has an impact on the integral since the exponential factor drops near zero for other flow regime. Table 1 lists the exponential factor range regarding different flow regime and Fig.9 demonstrate the effective drainage volume calculated by the integral.

Flow Regime	Exponential Range	Boltzmann Variable Range
Pseudo-Steady State	$e^{-\tau^2/4t} > 0.99$	$\xi < 0.01$
Approximate PSS	$0.99 > e^{-\tau^2/4t} > 0.9$	$0.01 < \xi < 0.1$
Transient	$0.9 > e^{-\tau^2/4t} > 0.018$	$0.1 < \xi < 4$
Near Initial	$e^{-\tau^2/4t} < 0.018$	$\xi > 4$

Table 1. Exponential Factor and Boltzmann Variable Range

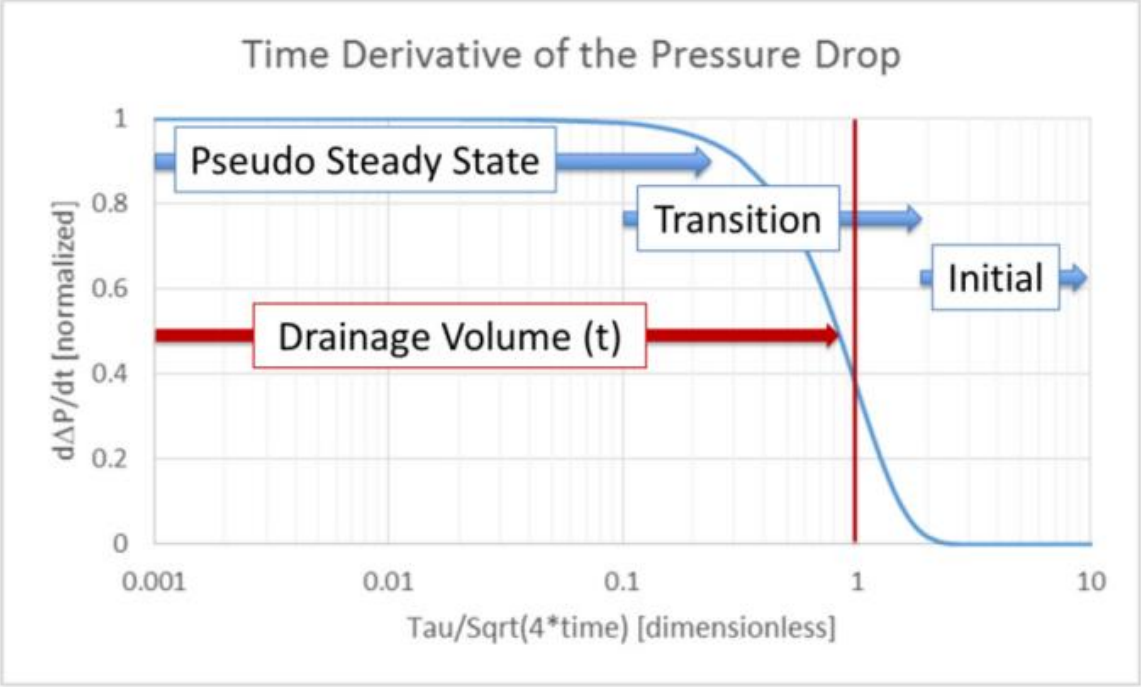

Fig.9 Flow Regime in Reservoir Regarding Different Boltzmann Variable Value (Reprinted from King *et al.* 2016)

Bourdet defined the well test derivative (Bourdet et al. 1983) as pressure derivative regarding logarithm time at the well. Therefore we can relate the well test derivative calculation to our asymptotic solution as

$$\Delta p'_{wf} = \frac{d\Delta p_{wf}}{d\ln t} = \frac{qt}{c_t V(t)} \tag{2.25}$$

Our main aim is to match the well test derivative with history data which indicates a correct calculation of drainage volume and calibrated reservoir model.

Eq.(2.25) is mostly efficient in Infinite Acting Radial Flow (IAFR). However, most reservoirs in real life contains boundary conditions. It is either a physical boundary at formation intersect or a virtual boundary created by well/fracture interference. In order for Eq.(2.25) to feel the boundary effect, when integrating for the drainage volume, every time the pressure diffusion reaches a boundary, the front shape changes, therefore the corresponding $w(\tau)$ has to change as well. We illustrate such behavior using a simple rectangle reservoir in Fig.10.

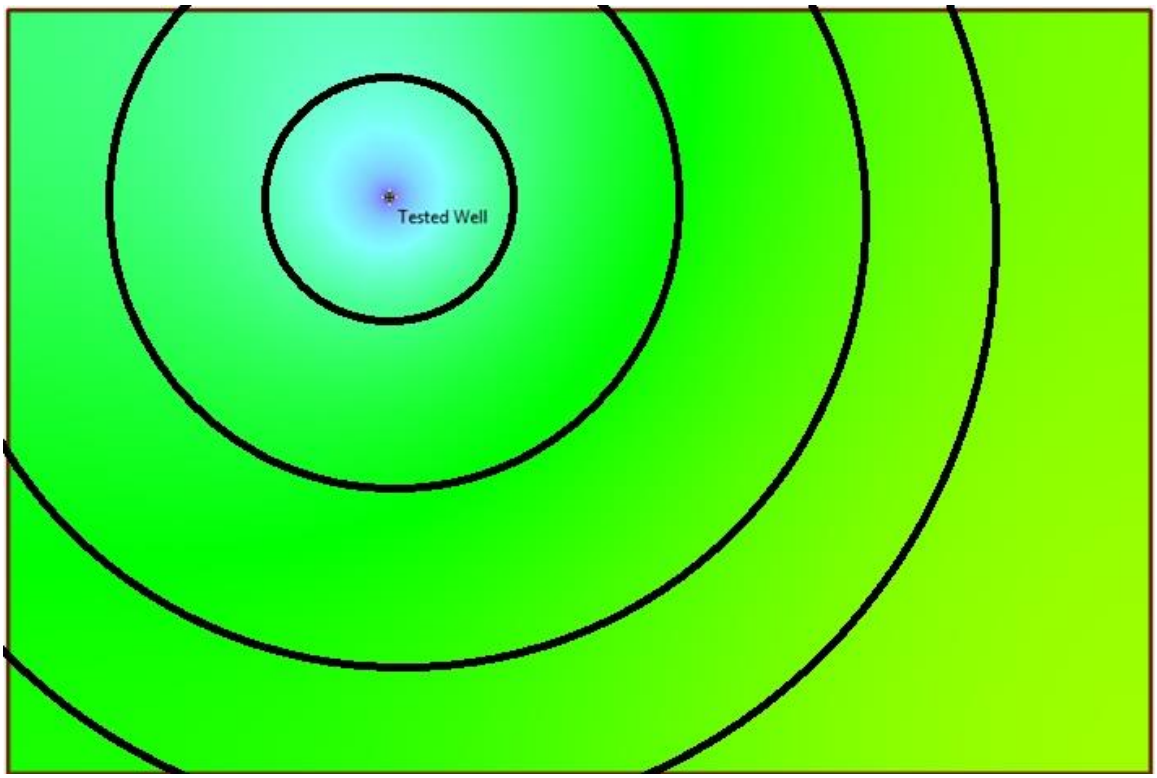

Fig.10 Pressure Front Shape Changes As Pressure Diffusion Reaches Boundary and Corner

The constantly changing $w(\tau)$ behavior makes the integral only achievable numerically since the front area becomes irregular after reaching the boundaries and the value for $w(\tau)$ term needs to be calculated step by step. The approach to calculate the irregular front area is to separate the circumference into a straight line segments and arc segments as demonstrated by Fig.11. We calculate the angle of each segment geometrically by knowing the distance to each boundary. The angle related with each segment provide us the segment length by using circle and trigonometric identities.

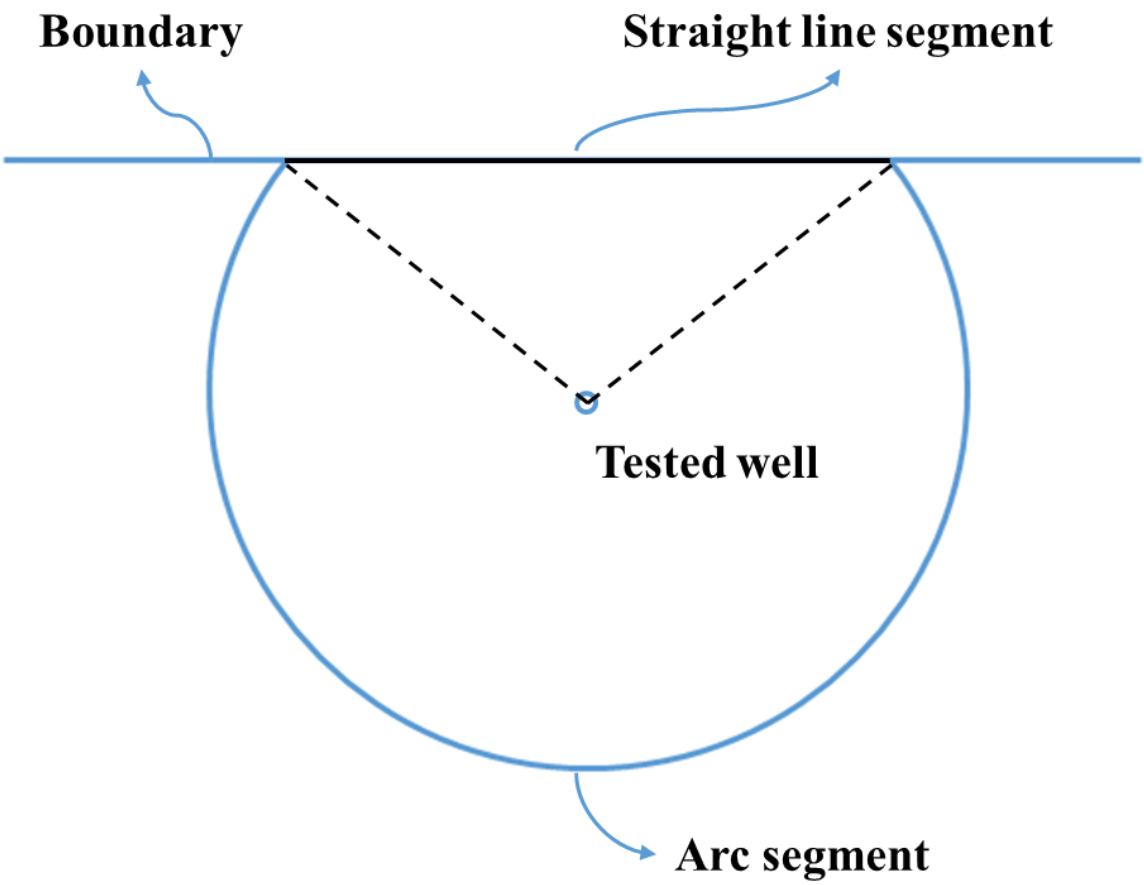

Fig.11 Calculate Front Shape Area Geometrically after Encountering Boundary Conditions

After obtaining the drainage volume by this approach, we compute the well test derivative and compare it against the reference result generated by Ecrin. The result is shown in Fig.12.

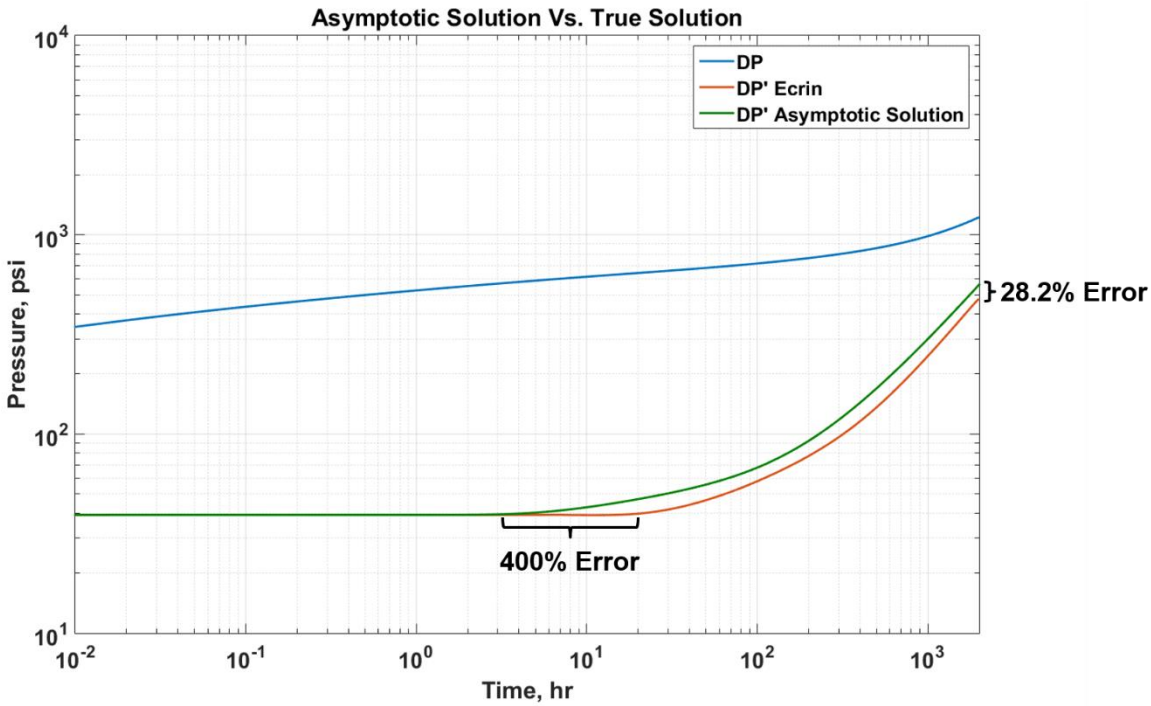

Fig.12 Well Test Derivative Calculated by Asymptotic Solution without Reflection and Transmission Mechanism Compared against Reference Solution Generated by Ecrin

We notice in the figure that the late time mismatch as an error of 28%. However this error should be diminished as we elongate the production time. However, the more significant error is spotted during the estimation of distance to the boundary. Behold that the time when the asymptotic solution curve starts to deviate from the IARF is 4 times earlier than the reference solution. The reason for this error is because to model the boundary conditions by changing the $w(\tau)$ expression, the well will feel the boundary as soon the pressure front reaches it. However, the well should only detect the boundary once the pressure front has traveled a round trip. A misinterpretation of distance by two times causes the response time to decrease by four times. This phenomenon confirms

that to model the boundaries with asymptotic solution, we need to incorporate the reflection and transmission mechanism.

Our asymptotic solution is derived by drawing upon the analogy between pressure diffusion and electromagnetic wave propagation, therefore the mechanism valid for electromagnetic wave is also applicable for pressure diffusion. When electromagnetic wave encounters boundary conditions, the interface of two media, part of it is reflected back to the same media while the remainder is transmitted to the other media. Such mechanism is illustrated in Fig.13. Pressure diffusion behave similarly when it reaches a boundary in the reservoir.

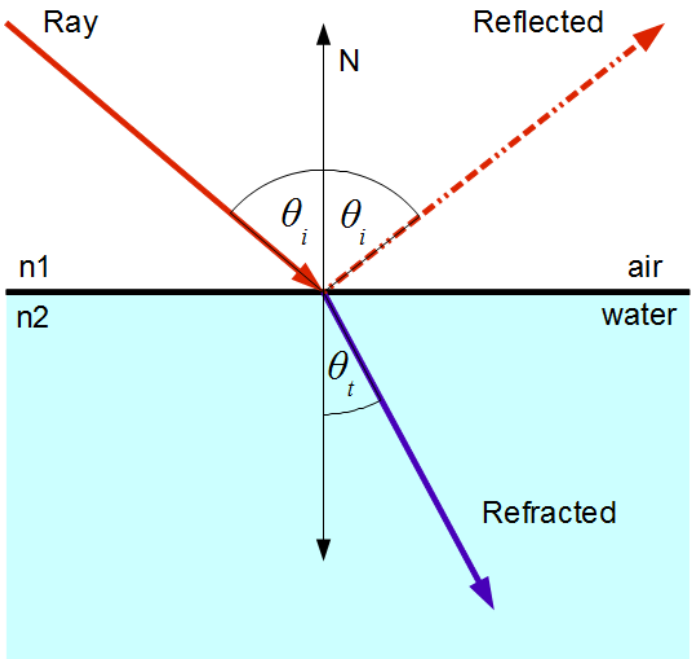

Fig.13 Reflection and Transmission Mechanism of Electromagnetic Wave Propagation

We incorporate the reflection and transmission mechanism into Eq.(2.23)

$$c_t \frac{\partial p(\tau,t)}{\partial t} = \frac{1}{w(\tau)} \frac{\partial q(\tau,t)}{\partial \tau} \approx -\frac{q_w}{V(t)} \begin{cases} e^{-\frac{\tau^2}{4t}} + R \cdot e^{-\frac{(2\tau_d - \tau)^2}{4t}} & (\tau \le \tau_d) \\ T \cdot e^{-\frac{\tau^2}{4t}} & (\tau > \tau_d) \end{cases} \tag{2.26}$$

In the above equation, R and T are the reflection and transmission coefficients, and τ_d is the DTOF at the boundary which governs the observation time of reflection and transmission of pressure diffusion. We can also incorporate such mechanism into the flux equation.

$$\frac{\partial q(\tau,t)}{\partial t} = w(\tau) \frac{\partial}{\partial \tau} \left(c_t \frac{\partial p(\tau,t)}{\partial t} \right) \approx \frac{q_w}{2tV(t)} \begin{cases} w(\tau) \cdot \left[\tau \cdot e^{-\frac{\tau^2}{4t}} - (2\tau_d - \tau) \cdot R \cdot e^{-\frac{(2\tau_d - \tau)^2}{4t}} \right] & \tau \le \tau_d \\ w(\tau) \cdot \left[T \cdot \tau \cdot e^{-\frac{\tau^2}{4t}} \right] & \tau > \tau_d \end{cases}$$

(2.27)

At the boundary conditions, there are always discontinuities created by sudden change of properties such as permeability and porosity. However, the pressure and flux time dependent derivatives are always continuous. Therefore, expressing the pressure and flux continuity at boundary conditions by Eq.(2.26) and Eq.(2.27) we have

$$\begin{cases} \left[\frac{\partial p}{\partial t} \right]_{\tau_d} = 0 & 1 + R = T \\ \left[\frac{\partial q}{\partial t} \right]_{\tau_d} = 0 & w(\tau)_{left} \cdot (1 - R) = w(\tau)_{right} \cdot T \end{cases} \tag{2.28}$$

This provides us the tool to solve for the actual values of reflection and transmission coefficient. At no flow boundaries as a special condition, the $w(\tau)_{right}$ increases to infinity. Therefore, the value for R and T at no flow boundaries are as follow.

$$\begin{cases} R = 1 \\ T = 2 \end{cases} \tag{2.29}$$

With the value of R and T, we integrate for the time dependent volume on both sides of the boundary separately.

$$V(t) = \int_0^{\tau_d} w(\tau) \cdot \left(e^{-\frac{\tau^2}{4t}} + R \cdot e^{-\frac{(2\tau_d - \tau)^2}{4t}} \right) \cdot d\tau + \int_{\tau_d}^{\infty} w(\tau) \cdot T \cdot e^{-\frac{\tau^2}{4t}} \cdot d\tau \tag{2.30}$$

Afterwards, the well test derivative calculation is given by

$$\Delta p'_{wf} = \frac{d\Delta p_{wf}}{d\ln t} = \frac{qt}{c_t V(t)} \left(1 + R \cdot e^{-\frac{\tau_d^2}{t}} \right) \tag{2.31}$$

We can include the exponential factor into the $V(t)$ term which gives rise to the actually drainage volume experienced at the well.

$$V_d(t) = \frac{V(t)}{1 + R \cdot e^{-\frac{\tau_d^2}{t}}} \tag{2.32}$$

While all the above derivations progressed under the assumption of fixed rate drawdown, most field produces with variable rate. In variable rate drawdown cases, we use rate normalized pressure derivative for analysis. Therefore Eq.(2.31) becomes

$$\Delta RNP' = \frac{d\Delta RNP}{d\ln(t_e)} = \frac{t_e}{c_t V_d(t)} \tag{2.33}$$

The time variable is changed to material balance time in variable rate drawdown cases. While this time is only completely valid after the reservoir has reached boundary dominated flow, it is still an accurate enough approximation for other flow regimes (Blasingame 1986).

We test the reflection and transmission methodology in the flow regime we are interested in, the channel flow. We constructed a channel reservoir with a vertical well not on the symmetrical center as demonstrated in Fig.14. The parameters used in this case are listed in Table 2.

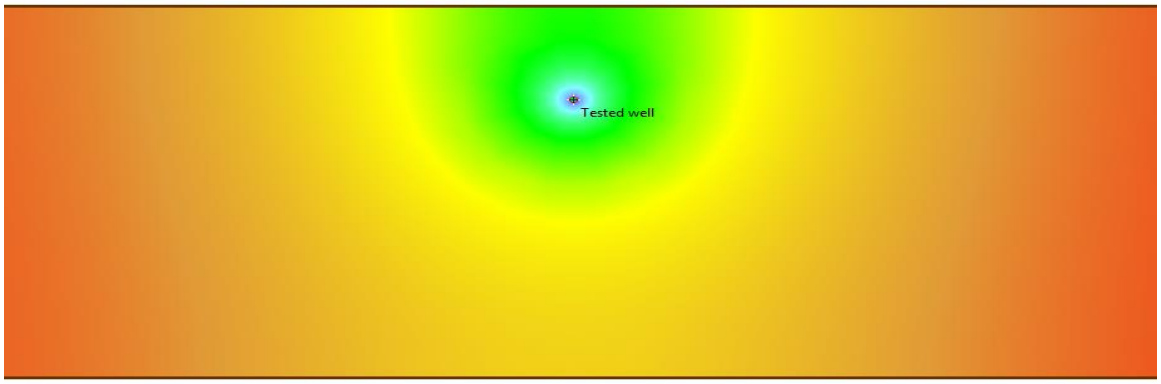

Fig.14 Channel Reservoir Used to Test Asymptotic Solution with Reflection and Transmission Mechanism

Thickness, ft	**50**
Porosity	**0.1**
Viscosity, cp	**0.3**
Compressibility, psi^{-1}	**3e-6**
Permeability, md	**50**
Production Rate, bbl/d	**500**
Production Time, hr	**1000**
North Boundary Distance, ft	**400**
South Boundary Distance, ft	**1000**

Table 2. Reservoir and Fluid Parameters for Channel Reservoir

We calculate the integral for time dependent volume geometrically using the method already demonstrated by Fig.11. After running the algorithm, the result is shown in Fig.15.

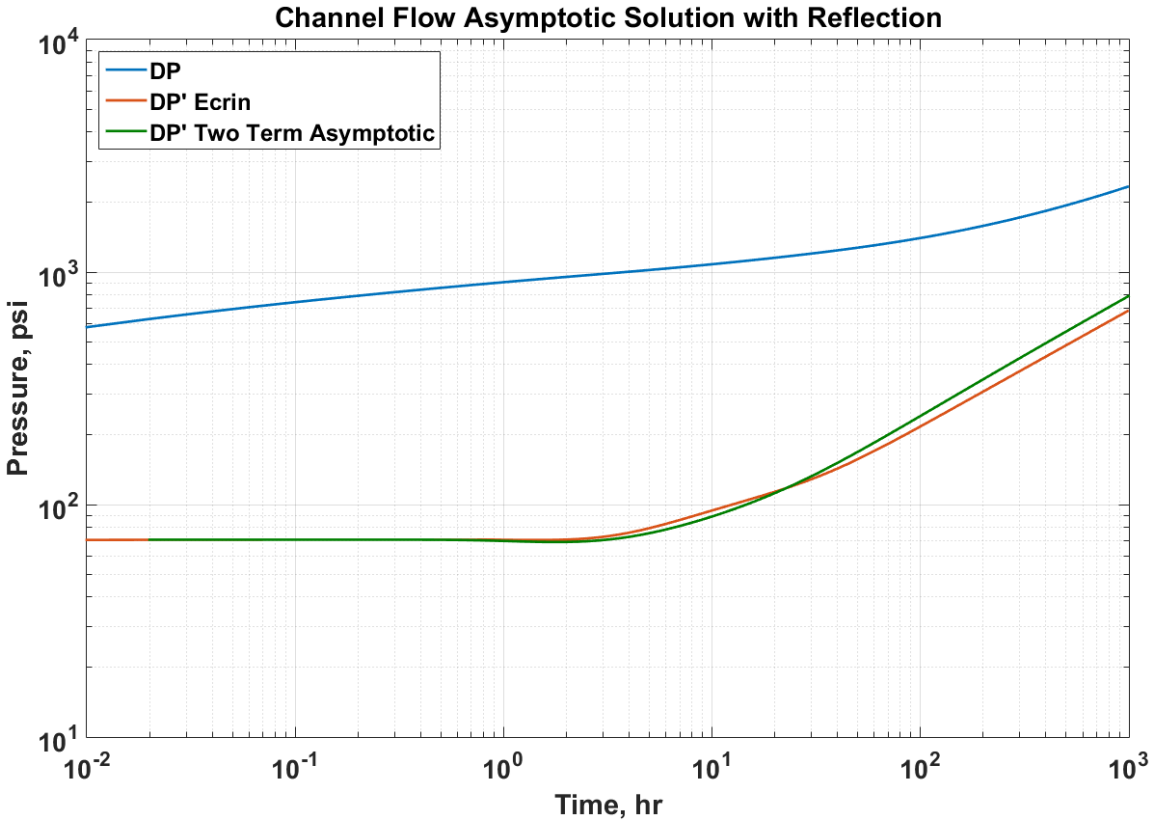

Fig.15 Well Test Derivative Calculated by Asymptotic Solution with Reflection and Transmission Mechanism Using Geometric Method Compared against Reference Solution Generated by Ecrin

We are aware from the plot that we have very accurate match during early time when the well is still in infinite acting radial flow (IARF) regime. The solution also captures the correct distance to the boundary as the two curves start to deviate from the flat portion at the same time. However the solution is not accurate during middle time (100 hour and after) since the two solutions does not overlap with each other.

2.3 Separation of Variables

The equation with reflection and transmission is very efficient in capturing circular no flow boundaries or composite reservoirs where we observe sudden change in diffusivity usually due to formation damage effect. The reason is that the pressure front arrives at the discontinuity at the same time and the front shape does not change. However, for linear directional boundaries, the front shapes changes continuously after the pressure diffusion has reached the boundary. For cases where parallel linear boundaries are present, the problem becomes even more tedious.

The main objective of this thesis is to model pressure and drainage behavior of multistage fractured horizontal wells so as to capture PPSS flow regime generally observed in unconventional reservoirs. The adjacent fractures create virtuous boundary effect by interfering with each other. Therefore, each fracture produces equivalently in a channel with parallel boundaries. The channel reservoir is characterized by pressure diffusion encountering boundaries in one direction but propagates infinitely in the perpendicular direction. Thus, capturing the pressure diffusion in two directions separately will return more accurate result on well test derivative. To do so, we need to change the algorithm of integration for drainage volume. Since all previous equations for drainage volume calculation are integrating in 1-D τ coordinate, our new methodology is to decompose this integral into X and Y directions which will represent the bounded and unbounded direction respectively. By decomposition, we are integrating in discretized rectangles instead of thin disks along τ contours as demonstrated in Fig.16.

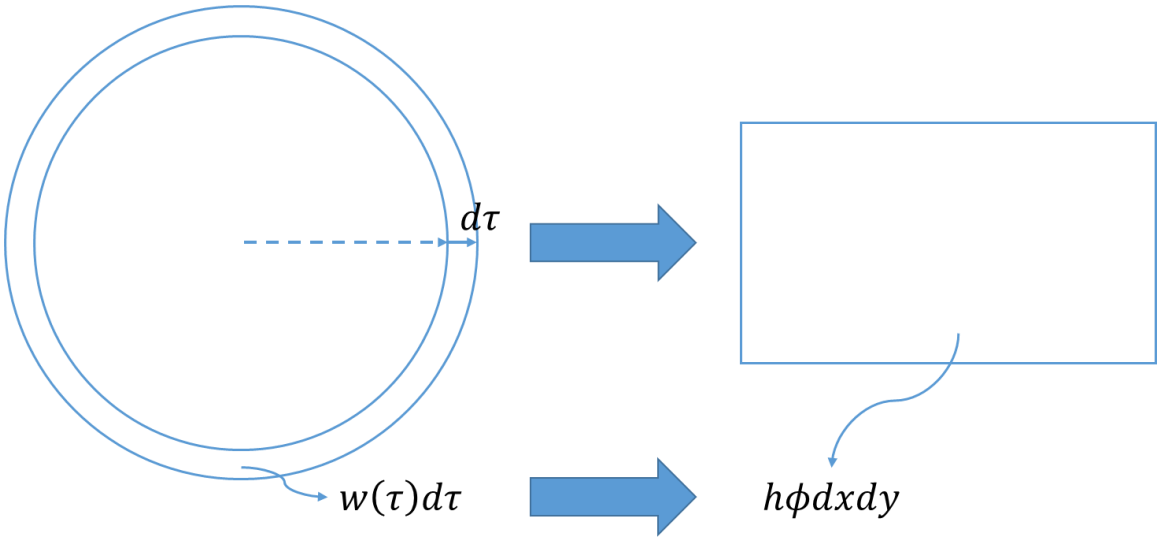

Fig.16 Transformation of Integration from 1-D τ Coordinate to Cartesian Coordinate

Let us start the derivation with the integration of a circle area using the radial coordinate.

$$A_{circle} = \int_0^r 2\pi r dr \tag{2.34}$$

Similarly, we can calculate the drainage volume in radial coordinate as

$$V(t) = \int_0^\infty h\phi(2\pi r)\cdot e^{-\frac{\phi\mu c_t r^2}{4kt}}\cdot dr \tag{2.35}$$

On the other hand, we can also calculate the circle area in Cartesian coordinate.

$$A_{circle} = 2\int_0^r \left(2\int_0^{\sqrt{r^2-y^2}} dx \right) dy \tag{2.36}$$

Therefore, our drainage volume integral Eq.(2.24) for vertical wells can be modified to

$$V(t)=\int_0^{\infty}\int_0^{\infty} h\phi\cdot\left(e^{-\frac{\phi\mu c_t x^2}{4kt}}\cdot e^{-\frac{\phi\mu c_t y^2}{4kt}}\right)\cdot dxdy \tag{2.37}$$

Instead of integrating to a certain value, the asymptotic solution integrates to infinity in both directions, making variables in X and Y directions independent of each other. Therefore, we can decouple the two integrals.

$$V(t)=h\phi\cdot\left(2\int_0^{\infty} e^{-\frac{\phi\mu c_t x^2}{4kt}}dx\right)\cdot\left(2\int_0^{\infty} e^{-\frac{\phi\mu c_t y^2}{4kt}}dy\right) \tag{2.38}$$

With Eq.(2.38), let's change the variables into τ system and incorporate boundary conditions in X and Y directions separately.

$$V_d(t)=h\phi\cdot\left\{2\left[\int_0^{\tau_{xd}}\sqrt{\frac{k}{\phi\mu c_t}}\left(e^{-\frac{\tau_x^2}{4t}}+R\cdot e^{-\frac{(2\tau_{xd}-\tau_x)^2}{4t}}\right)d\tau_x+\int_{\tau_{xd}}^{\infty}\sqrt{\frac{k}{\phi\mu c_t}}\left(T\cdot e^{-\frac{\tau_x^2}{4t}}\right)d\tau_x\right]\Big/\left(1+R\cdot e^{-\frac{\tau_{xd}^2}{t}}\right)\right\}$$
$$\cdot\left\{2\left[\int_0^{\tau_{yd}}\sqrt{\frac{k}{\phi\mu c_t}}\left(e^{-\frac{\tau_y^2}{4t}}+R\cdot e^{-\frac{(2\tau_{yd}-\tau_y)^2}{4t}}\right)d\tau_y+\int_{\tau_{yd}}^{\infty}\sqrt{\frac{k}{\phi\mu c_t}}\left(T\cdot e^{-\frac{\tau_y^2}{4t}}\right)d\tau_y\right]\Big/\left(1+R\cdot e^{-\frac{\tau_{yd}^2}{t}}\right)\right\} \tag{2.39}$$

If assume no flow boundary condition, then we simplify Eq.(2.39) to

$$V_d(t)=h\phi\cdot\left\{2\int_0^{\tau_{xd}}\sqrt{\frac{k}{\phi\mu c_t}}\left(e^{-\frac{\tau_x^2}{4t}}+e^{-\frac{(2\tau_{xd}-\tau_x)^2}{4t}}\right)d\tau_x\Big/\left(1+e^{-\frac{\tau_{xd}^2}{t}}\right)\right\}$$
$$\cdot\left\{2\int_0^{\tau_{yd}}\sqrt{\frac{k}{\phi\mu c_t}}\left(e^{-\frac{\tau_y^2}{4t}}+e^{-\frac{(2\tau_{yd}-\tau_y)^2}{4t}}\right)d\tau_y\Big/\left(1+e^{-\frac{\tau_{yd}^2}{t}}\right)\right\} \tag{2.40}$$

Eq.(2.40) assumes the boundaries are symmetrical regarding the well location. If such assumption is not satisfied, then the integral must be expanded as follow.

$$V_d(t) = h\phi \cdot \left\{ \begin{array}{l} \int_0^{\tau_{xd1}} \sqrt{\frac{k}{\phi\mu c_t}} \left(e^{-\frac{\tau_x^2}{4t}} + e^{-\frac{(2\tau_{xd1}-\tau_x)^2}{4t}} \right) d\tau_x \Big/ \left(1 + e^{-\frac{\tau_{xd1}^2}{t}} \right) + \\ \int_0^{\tau_{xd2}} \sqrt{\frac{k}{\phi\mu c_t}} \left(e^{-\frac{\tau_x^2}{4t}} + e^{-\frac{(2\tau_{xd2}-\tau_x)^2}{4t}} \right) d\tau_x \Big/ \left(1 + e^{-\frac{\tau_{xd2}^2}{t}} \right) \end{array} \right\}$$
$$\cdot \left\{ \begin{array}{l} \int_0^{\tau_{yd1}} \sqrt{\frac{k}{\phi\mu c_t}} \left(e^{-\frac{\tau_y^2}{4t}} + e^{-\frac{(2\tau_{yd1}-\tau_y)^2}{4t}} \right) d\tau_y \Big/ \left(1 + e^{-\frac{\tau_{yd1}^2}{t}} \right) + \\ \int_0^{\tau_{yd2}} \sqrt{\frac{k}{\phi\mu c_t}} \left(e^{-\frac{\tau_y^2}{4t}} + e^{-\frac{(2\tau_{yd2}-\tau_y)^2}{4t}} \right) d\tau_y \Big/ \left(1 + e^{-\frac{\tau_{yd2}^2}{t}} \right) \end{array} \right\} \tag{2.41}$$

We move forward to validate the methodology of using separation of variables to represent boundary conditions using the previous channel case. Considering the well is not placed symmetrically in the channel, the equation applicable for this situation is Eq.(2.41). We apply boundary conditions in y direction while leaving x direction infinite acting. For this case, we will only use two exponential terms (original out going exponential and one reflection exponential). The result is illustrated in Fig.17.

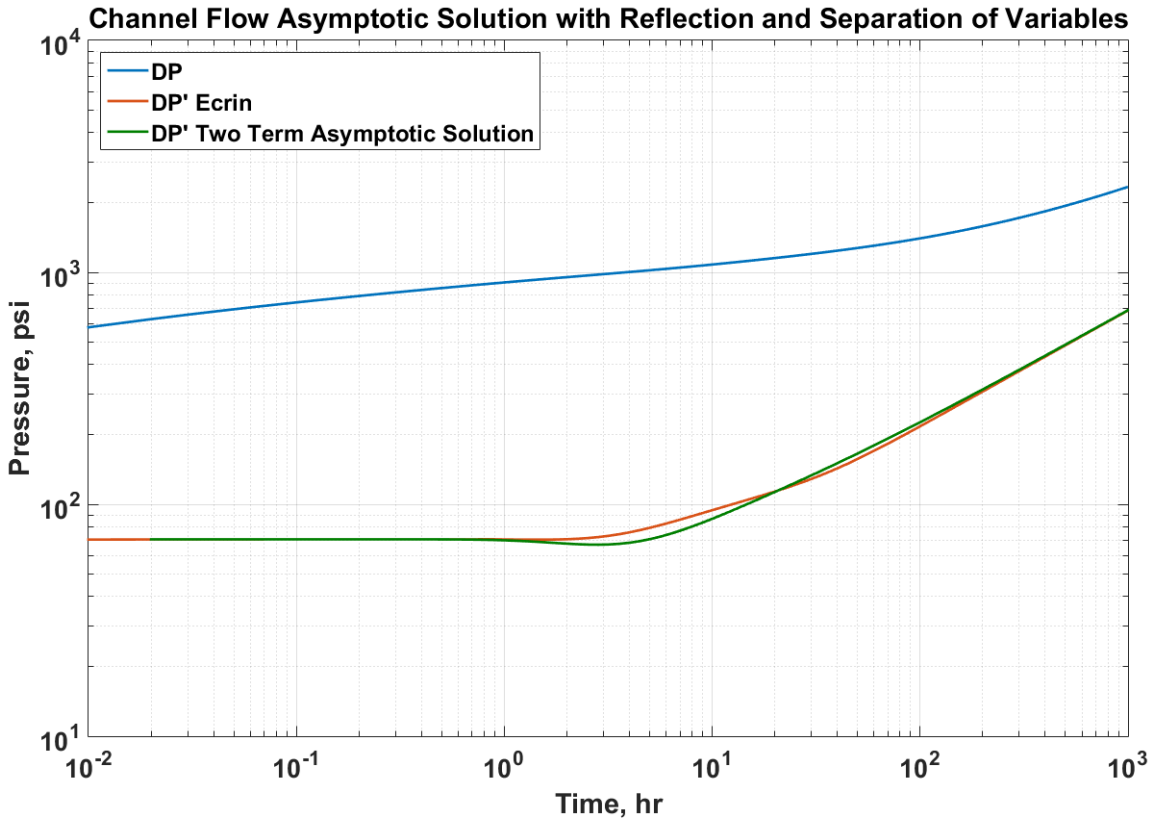

Fig.17 Well Test Derivative Calculated by Asymptotic Solution with Reflection and Transmission Mechanism Using Separation of Variables Method (Two Terms) Compared against Reference Solution Generated by Ecrin

The above result indicates that we have captured the general behavior of pressure diffusion in a channel reservoir, including early time, middle time and distance to the boundary. However, we still observe some mismatch and we want to minimize it as much as possible.

2.4 Infinite Series

Let us restate the previous flux equation by $w(\tau)$ formulation with no flow boundaries.

$$\frac{\partial q(\tau,t)}{\partial t}=\frac{q_w}{2tV(t)}\cdot w(\tau)\cdot\left[\tau\cdot e^{-\frac{\tau^2}{4t}}-(2\tau_d-\tau)\cdot e^{-\frac{(2\tau_d-\tau)^2}{4t}}\right] \tag{2.42}$$

We impose fixed rate drawdown at the well, therefore $\frac{\partial q(\tau=0,t)}{\partial t}=0$. However, when substituting $\tau=0$ into Eq.(2.42), the flux time dependent derivative is non-zero after the reflection exponential becomes influential. In order for the equation to be valid, we must implement another reflection term to the above flux equation to counteract the pressure reflection coming from the boundary.

$$\frac{\partial q(\tau,t)}{\partial t}=\frac{q_w}{2tV(t)}\cdot w(\tau)\cdot\left[\tau\cdot e^{-\frac{\tau^2}{4t}}-(2\tau_d-\tau)\cdot e^{-\frac{(2\tau_d-\tau)^2}{4t}}+(2\tau_d+\tau)\cdot e^{-\frac{(2\tau_d+\tau)^2}{4t}}\right]$$

(2.43)

However, this new additional term needs to be canceled at the no flow boundary. Consequently, we obtain an infinite serious of reflection terms. The time dependent volume integration using infinite series is

$$V(t)=\int_0^{\tau_d} w(\tau)\cdot\left(e^{-\frac{\tau^2}{4t}}+e^{-\frac{(2\tau_d-\tau)^2}{4t}}+e^{-\frac{(2\tau_d+\tau)^2}{4t}}+e^{-\frac{(4\tau_d-\tau)^2}{4t}}+e^{-\frac{(4\tau_d+\tau)^2}{4t}}+\cdots\right)\cdot d\tau \tag{2.44}$$

Accordingly the actually drainage volume of the well is

$$V_d(t)=\frac{V(t)}{1+2e^{-\frac{\tau_d^2}{t}}+2e^{-\frac{4\tau_d^2}{t}}+\cdots} \tag{2.45}$$

Maintaining the constant rate drawdown condition at the well is more important since our observation point is at the well. Therefore, we always use odd number of exponential terms in our formulation to represent reflections.

We use the previous channel case to investigate how many reflection terms are enough to calculate an accurate well test derivative and minimize the error we observed in Fig.17. We run the algorithm with one to five exponential terms and compare their drainage volume and well test derivative result in Fig.18 and Fig.19.

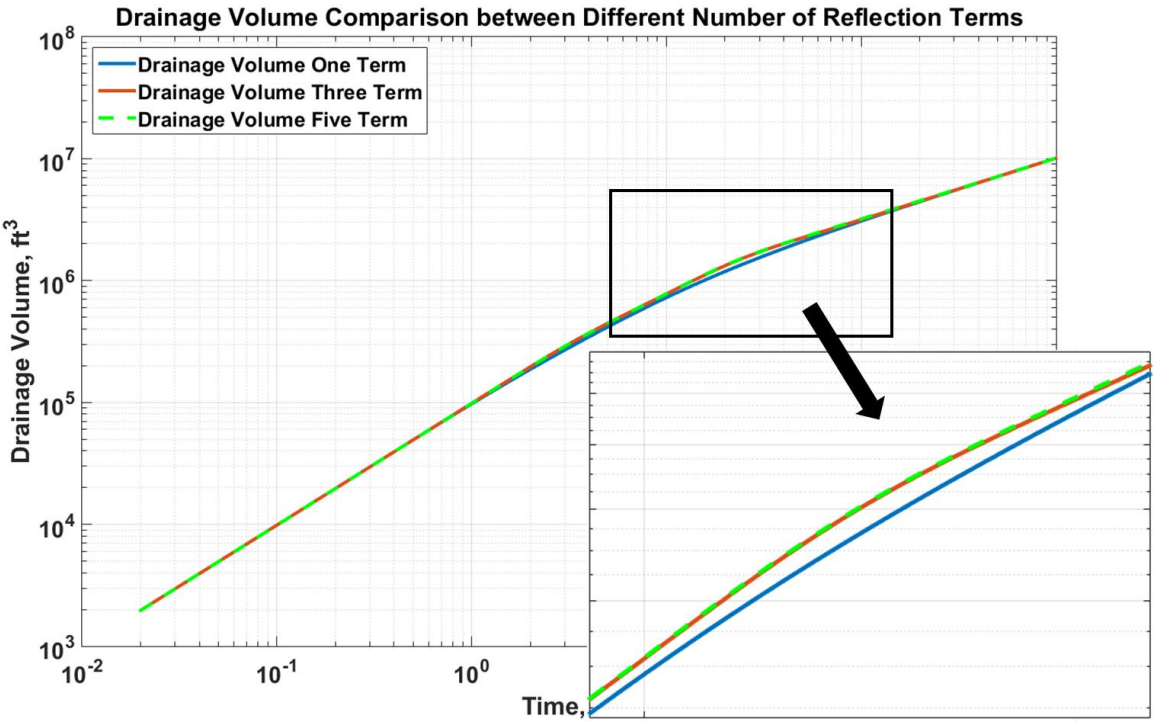

Fig.18 Drainage Volume Calculated with Different Number of Reflection Terms Comparison Indicates Three Terms Formulation is Optimum

The above comparison indicates that using no reflection term (one term curve) underestimates the drainage volume. However, we also notice the drainage volume curves generated by three and five terms overlap with each other, indicating that three term formulation (one outgoing exponential term from the well and two reflection exponential terms) is accurate enough to model boundary conditions using asymptotic

solution. Using more than three exponential terms simply increases the calculation load with barely no improvement on result.

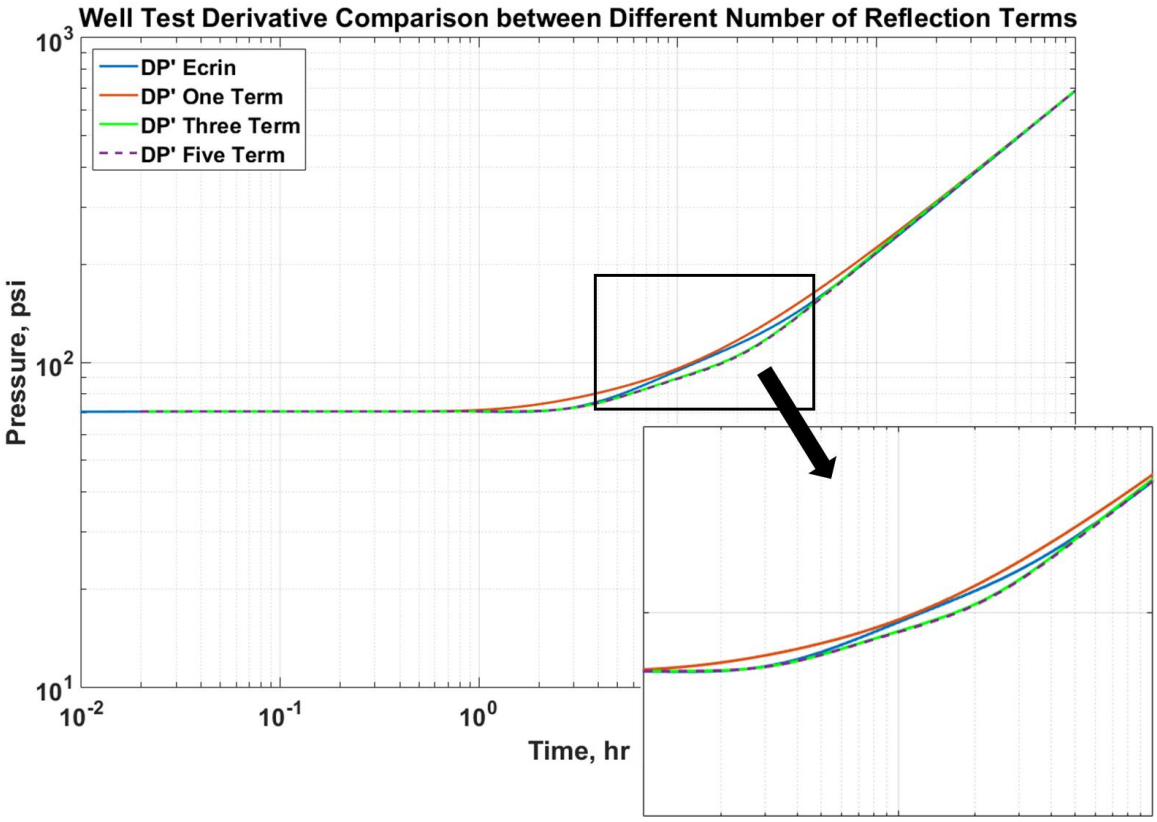

Fig.19 Well Test Derivative Calculated with Different Number of Reflection Terms Comparison Indicates Three Terms Formulation is Optimum

The plot of well test derivative infers the same statement. With the blue curve as the reference true solution generated by Ecrin, one term curve underestimates the distance to the boundary since the curve deviates from IARF earlier than the true solution.

After determining the optimum number of exponential terms to apply in the asymptotic solution formulation, we re-run the channel case and the optimum result is plotted in Fig.20.

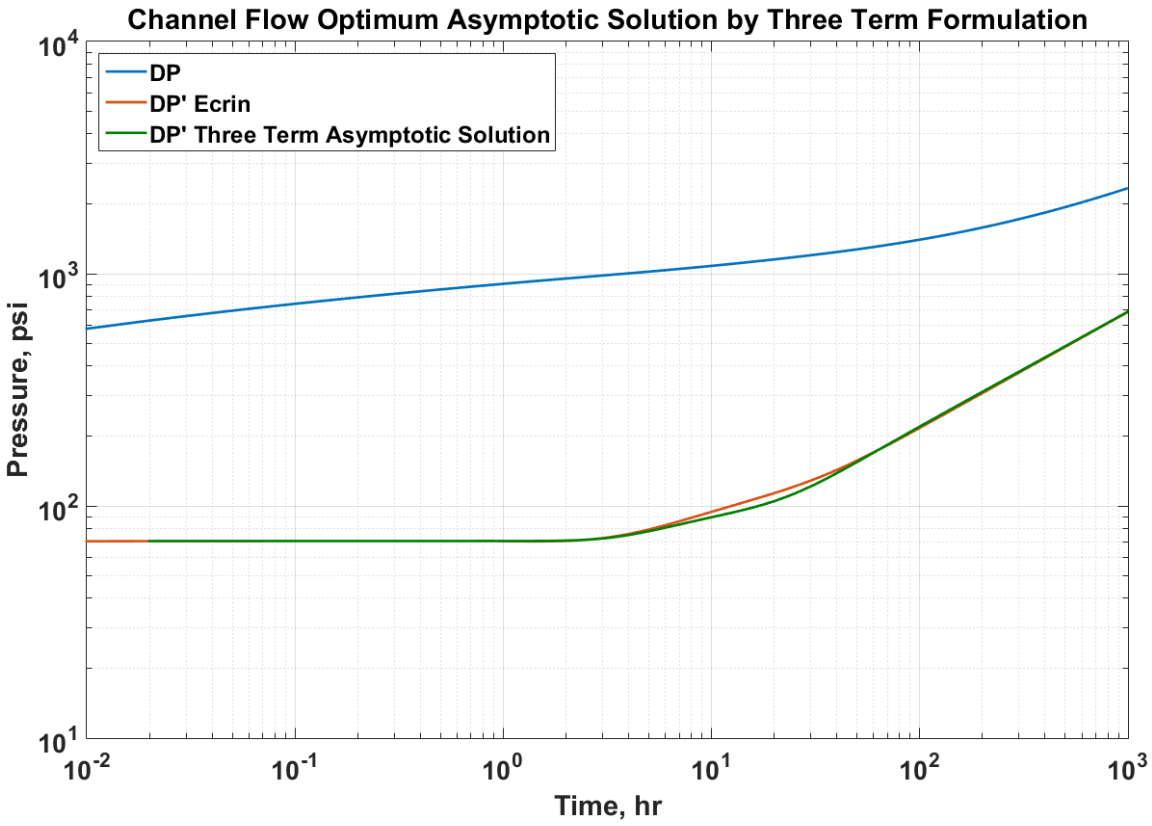

Fig.20 Well Test Derivative Calculated with One Outgoing Exponential Term and Two Reflection Terms Compared to Reference Solution Shows Minimum Mismatch

We discern that even with the mismatch minimized, there is still a slight separation between the two solution curves soon after the detection of boundary condition. This may due to the pressure contour shifting away from DTOF contour. However, since this slight separation does not affect the estimation of permeability (by early time well test

derivative), distance to the boundary (by the time when well test derivative deviates from IARF) and middle time pressure behavior, it is not necessary to correct it.

Calculating the drainage volume with the separation of variable method also enables us to capture the pressure diffusion distance is both X and Y directions since the equation constitutes two separate integrals. We can use this result shown in Fig.21 to double check the correctness of the methodology.

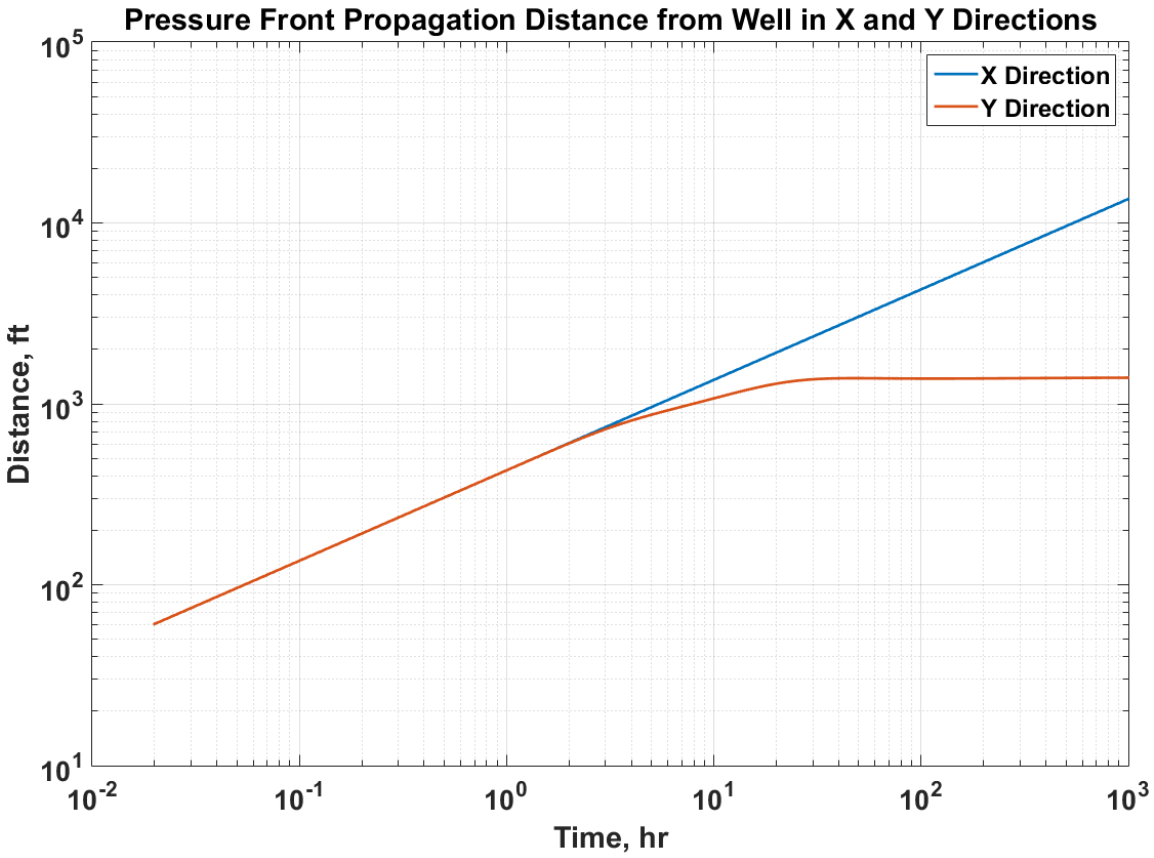

Fig.21 Pressure Front Propagation Distance from the Well in Both X and Y Directions Calculated by Separation of Variables Method

The plot shows that the pressure disturbance propagates in X direction linearly on a log-log scale since we did not impose any boundary conditions in that direction. However for Y direction, the pressure propagation starts linearly. Afterwards, it deviates and stabilizes around 1400 feet which is our channel width according to Table 2. Such result confirms that our methodology is valid.

2.5 Fracture Case Formulation

The final goal is to model the PPSS pressure behavior created by hydraulic fracture interference. Therefore, we also want to derive the separation of variable equation for fracture cases. In such scenario, the pressure propagates from the tip of the fracture and also along the fracture. The fracture half-length has to be included in the integral for one direction. The equation without boundary condition is stated as follow.

$$V(t) = h\phi \cdot \left(2\int_0^\infty \sqrt{\frac{k}{\phi\mu c_t}} e^{-\frac{\tau_x^2}{4t}} d\tau_x \right) \cdot \left[2\left(\int_0^\infty \sqrt{\frac{k}{\phi\mu c_t}} e^{-\frac{\tau_y^2}{4t}} d\tau_y + x_f \right) \right] \tag{2.46}$$

Eq.(2.46) is developed relying on the assumption that pressure contour is align with DTOF contour as a pill box. This assumption is only valid during very early time. Later, the actual pressure shape will shift towards ellipse. Corresponding to this problem, we need a correcting shape factor developed as follow.

$$A_{pillbox} = \pi r^2 + 4x_f r \tag{2.47}$$

$$A_{ellipse} = \pi\left(x_f + r\right) r \tag{2.48}$$

When $x_f \gg r$, the shape factor is calculated as

$$\frac{A_{pillbox}}{A_{ellipse}} = \frac{\pi r^2 + 4x_f r}{\pi r^2 + \pi x_f r} = \frac{4}{\pi} \tag{2.49}$$

In the next chapter, we will analyze cases with multiple fractures and the boundary condition created by fracture interference incorporated in the X direction. We will also analyze the effect of the shape factor.

CHAPTER III

HOMOGENEOUS MODEL DEMONSTRATION

In this chapter, we will discuss the result from several fracture cases in homogeneous reservoir. We will examine both single fracture and multiple fracture cases. The main goal is to simulate the PPSS flow regime. Based on the findings, we will proceed into heterogeneous reservoir in the next chapter.

3.1 Single Fracture Producing at Fixed Rate in Homogeneous Reservoir

After testing the validity of the separation of variables method in vertical well case, we move on to the next scenario, single fracture producing in a homogeneous reservoir. This scenario has a closer resemblance to the main objective of our research which is to model virtual boundary effects created by fracture interference and model PPSS flow regime. In this scenario we will calculate the drainage volume both analytically and semi-analytically. The semi-analytical method is a combination of Fast Marching Method (FMM) and asymptotic solution. We provide a discretized grid system with reservoir properties and use the FMM to solve for the diffusive time of flight (DTOF) for each grid block. Then we use the DTOF to calculate the drainage volume for each grid block. Finally, the summation of individual grid block drainage volume yields the total drainage volume. To complete the separation of variables calculation semi-analytically, we need to calculate the τ_x and τ_y term at each grid block. The τ_x and τ_y

relation to the total DTOF at specific grid block in homogeneous system is demonstrated in Fig.22 for vertical well and fracture cases.

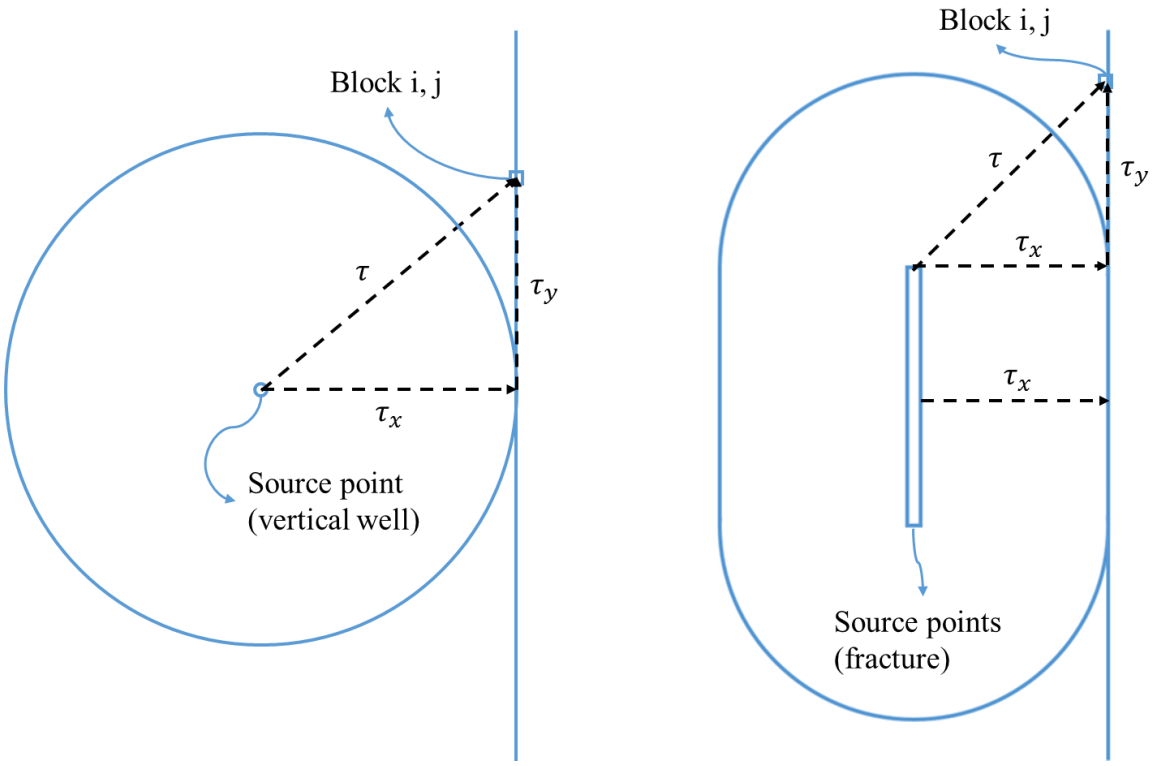

Fig.22 X and Y Direction DTOF Decomposition from Total DTOF for Vertical Well and Fracture Case

Such geometric decomposition resulted in a constant τ_{dx} value along the boundary.

The reservoir parameters we use in this case are listed in Table 3.

Porosity	**0.076**
Viscosity, cp	**0.2**
Compressibility, psi^{-1}	**3e-5**
Permeability, md	**0.1**
Production Rate, bbl/d	**10**
Production Time, hr	**10000**
DX, DY, DZ, ft	**10**
NX	**200**
NY	**101**
NZ	**1**
x_f, ft	**200**

Table 3. Reservoir Dimensions and Properties for a Single Fracture in Homogeneous Media

Apart from conducting the calculation either analytically and semi-analytically, we also input these parameters into Eclipse and use the numerical simulator to generate our reference solution. The reason we choose Eclipse this time is to prepare for analyzing heterogeneous cases in the future. The result for drainage volume and well test derivative is shown in Fig.23 and Fig.24.

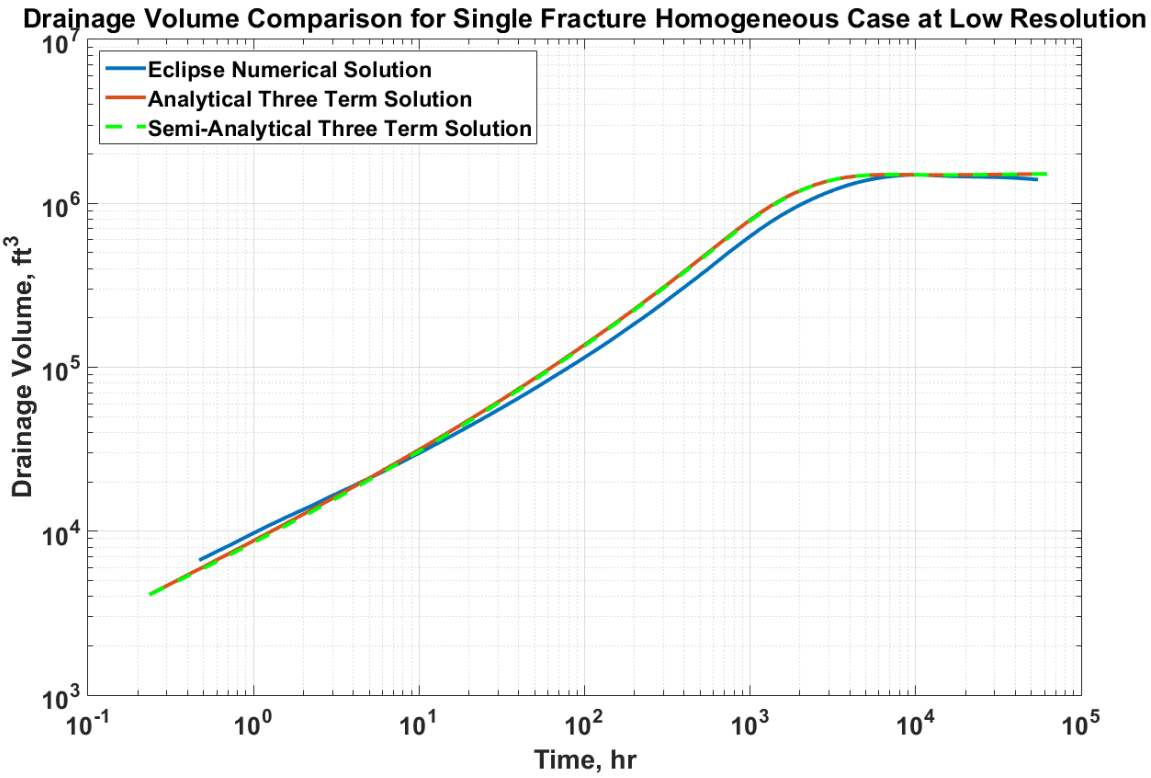

Fig.23 Drainage Volume Calculated by Asymptotic Solution with Separation of Variables (Analytical), Asymptotic Solution with Separation of Variables Plus FMM (Semi-Analytical) and Numerical Solution (Eclipse)

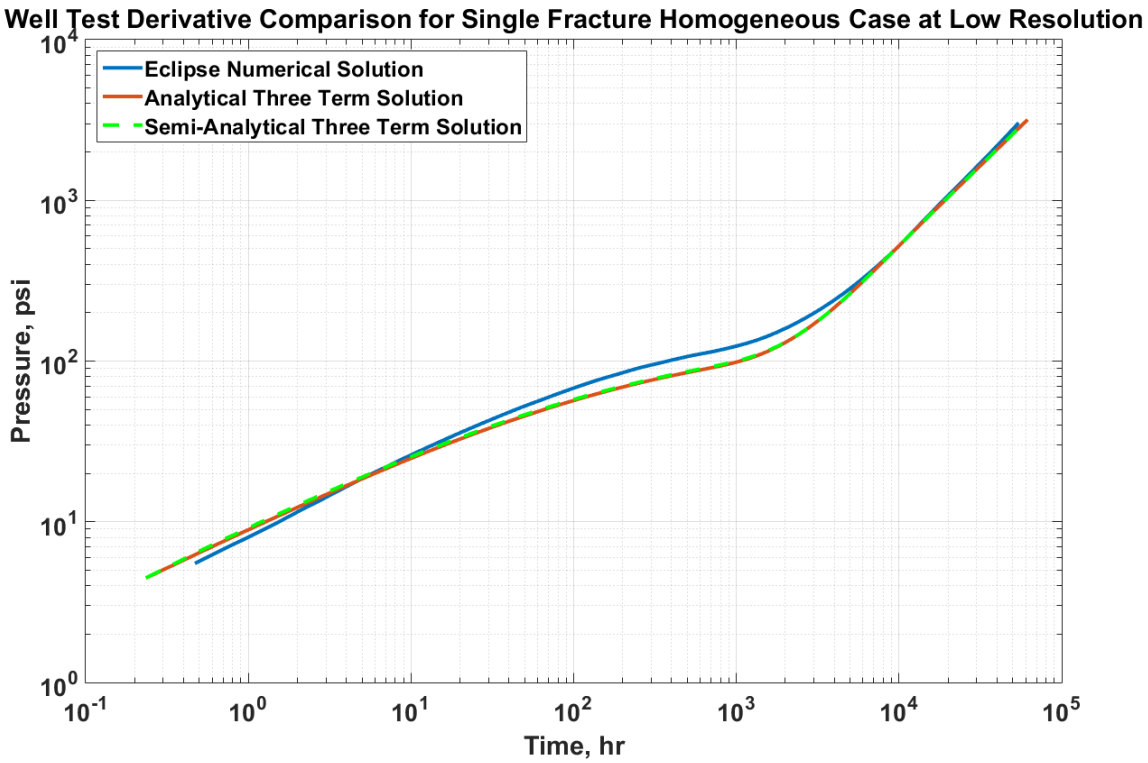

Fig.24 Well Test Derivative Calculated by Asymptotic Solution with Separation of Variables (Analytical), Asymptotic Solution with Separation of Variables Plus FMM (Semi-Analytical) and Numerical Solution (Eclipse)

The FMM considers the fracture as a group of source points. To be more specific, the fractures are assumed to have infinite conductivity. Therefore in order to simulate infinite conductivity fractures in Eclipse, we have to significantly increase the permeability of fracture grid blocks. This method introduces some error at low reservoir resolution when the grid block size is large. Correspondingly, we observe the Eclipse curve not strictly following one half slope during the early time. Soon after the early time, the analytical and semi-analytical results for the well test derivative and the drainage volume start to deviate from the numerical solution. The reason is because the DTOF calculated by FMM remains in a pill box contour even at late time. However, the

pressure front transform from pill box shape to ellipse shape rapidly according to Eclipse simulation. The comparison is shown in Fig.25.

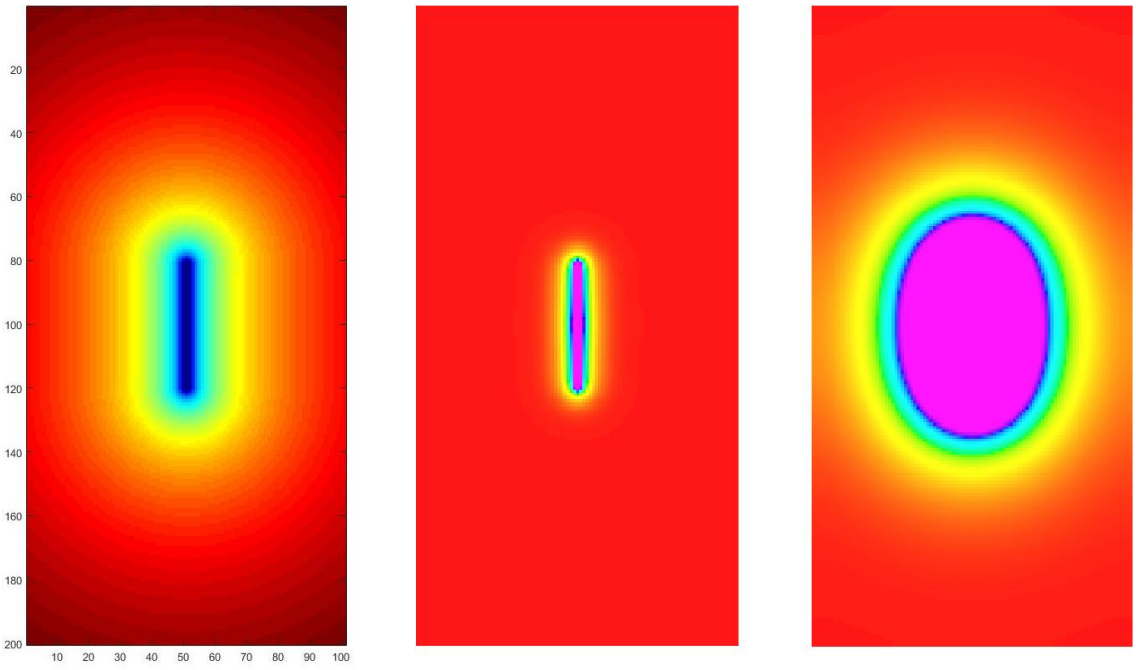

Fig.25 Comparison between DTOF Contours (Left), Early Time Pressure Diffusion Shape (Middle) and Middle Time Pressure Diffusion Shape (Right)

The asymptotic solution is developed based on the assumption that the pressure contour is nearly identical to the DTOF contour. And the difference in contour results in the overestimation of drainage volume and underestimation of well test derivative. Also the diffusion from the tip of the fracture is slower than the diffusion starting along the fracture. The numerical simulator captures such behavior while the asymptotic solution ignores it. This results in our solution sensing the boundary in Y direction earlier than the reference solution. After the pressure diffusion filled the entire reservoir and

stabilized, the well test derivative and drainage volume curves collapse together again. Since the early time error in Eclipse solution curve is most likely caused by the low grid resolution. The result from a higher grid resolution is presented in the following two graphs.

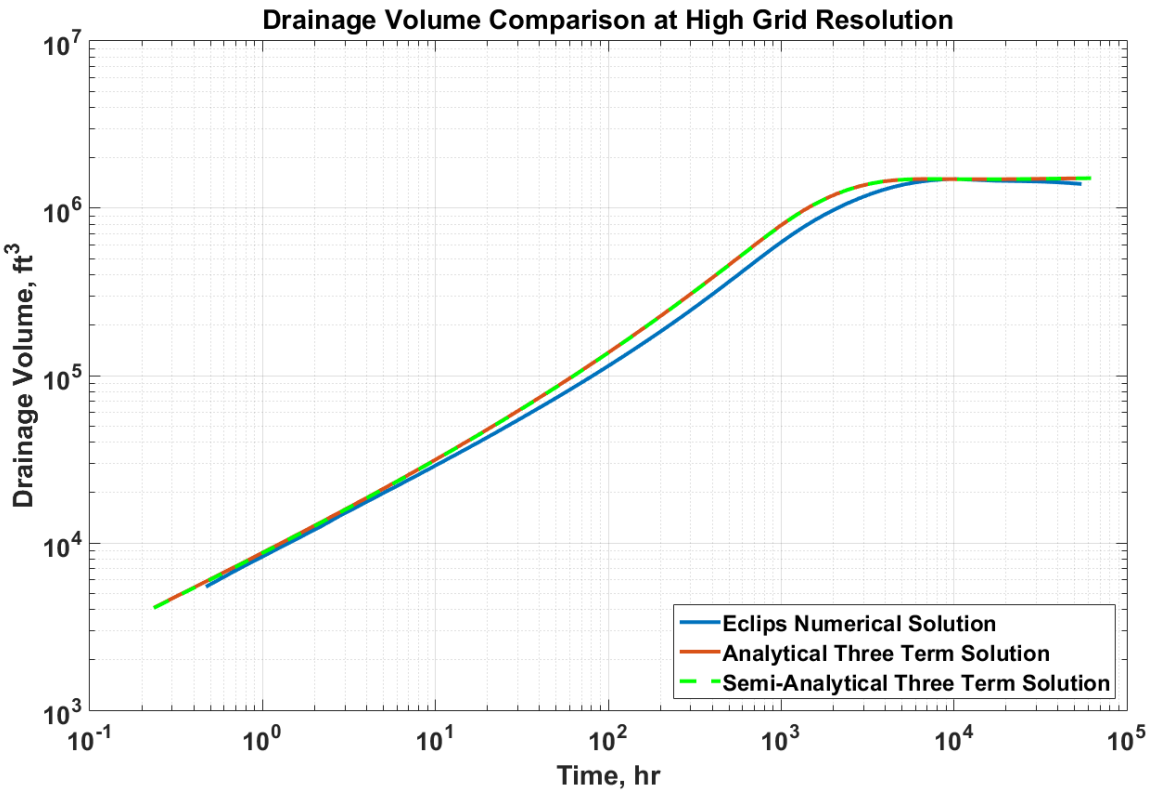

Fig.26 Drainage Volume Calculated by Asymptotic Solution with Separation of Variables (Analytical), Asymptotic Solution with Separation of Variables Plus FMM (Semi-Analytical) and Numerical Solution (Eclipse) at Higher Grid Resolution

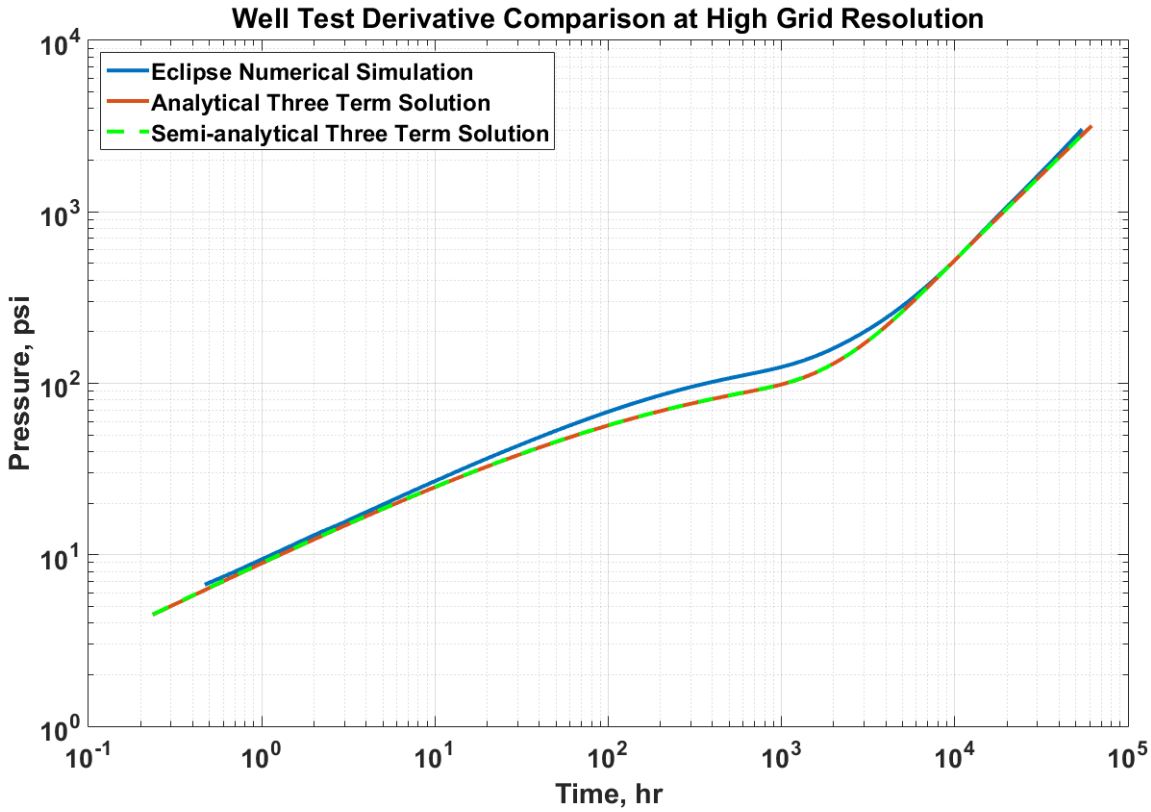

Fig.27 Well Test Derivative Calculated by Asymptotic Solution with Separation of Variables (Analytical), Asymptotic Solution with Separation of Variables Plus FMM (Semi-Analytical) and Numerical Solution (Eclipse) at Higher Grid Resolution

After refining the grid, the Eclipse early time solution becomes reasonable. However, the early time still have very small offset. This is due to the shape difference between the eclipse and pill box. We will correct this mismatch with a shape factor derived in Eq.(2.49) for our future cases.

3.2 Multiple Fracture with Tight Spacing Producing in Homogeneous Reservoir at Fixed Rate

Even though the analytical curves are deviating from the reference solution, the overall shapes of the curves are generally the same. This indicates that the analytical and semi-analytical methods still capture the correct feature of the reservoir. With this discovery, we want to proceed to the main goal of this research, to model pseudo pseudo-steady state flow with our solution. This flow regime occurs when there's a sudden significant loss of cross flow area. To simulate such situation, the next case we are going to investigate is a multiple fracture reservoir with very tight spacing.

We maintain some reservoir parameters from the previous case. All the parameters with new value are listed in Table 4.

Permeability, md	**0.01**
Production Rate, bbl/d	**0.05**
Production Time, days	**10000**
DX, DY, DZ, ft	**1**
NX	**2000**
NY	**121**
NZ	**1**
x_f, ft	**300**
Fracture Spacing, ft	**30**

Table 4. Reservoir Dimensions and Properties for Multiple Fractures in Homogeneous Media

We conduct the calculation using the semi-analytical method and compare it against the reference solution generated by Eclipse. The semi-analytical method uses the geometric decomposition illustrated by Fig.22 to calculate τ_x and τ_y. Using this decomposition method, we generated the map of the DTOF in two directions as illustrated in Fig.28.

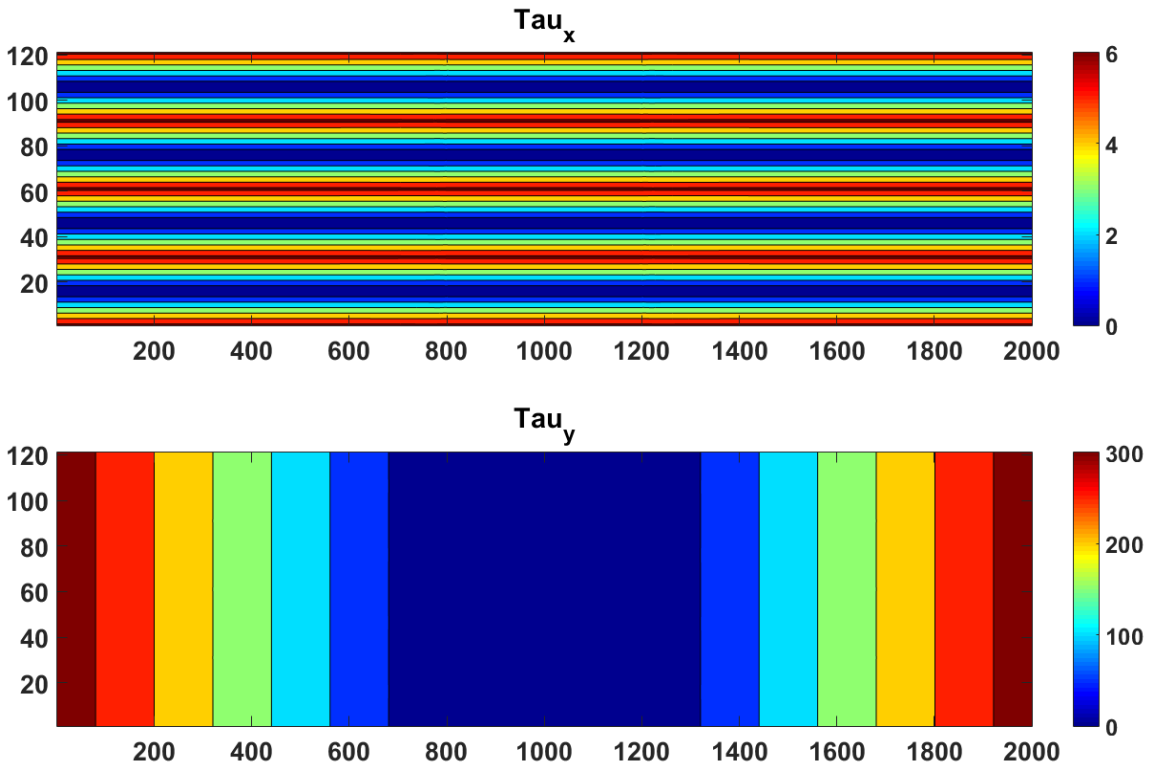

Fig.28 Decomposed Diffusive Time of Flight in X and Y Directions for Homogeneous Case

The decomposition map shows that the τ_x and τ_y are constant along boundaries in homogeneous reservoir. Using the directional DTOF, we calculate the drainage volume in order to obtain the well test derivative. A sample drainage volume map calculated by

the semi-analytical method with reflection and transmission mechanism is illustrated in Fig.29.

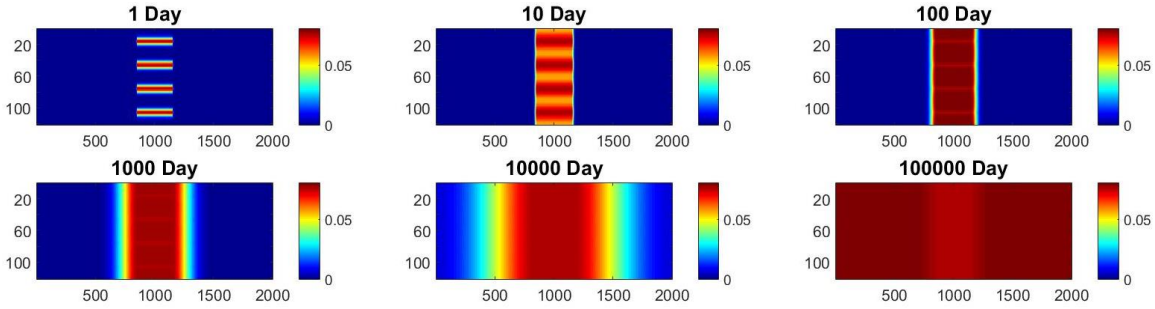

Fig.29 Drainage Volume Map at Different Time Point Calculated with Reflection and Transmission Mechanism

The well test derivative result is plotted in Fig.30.

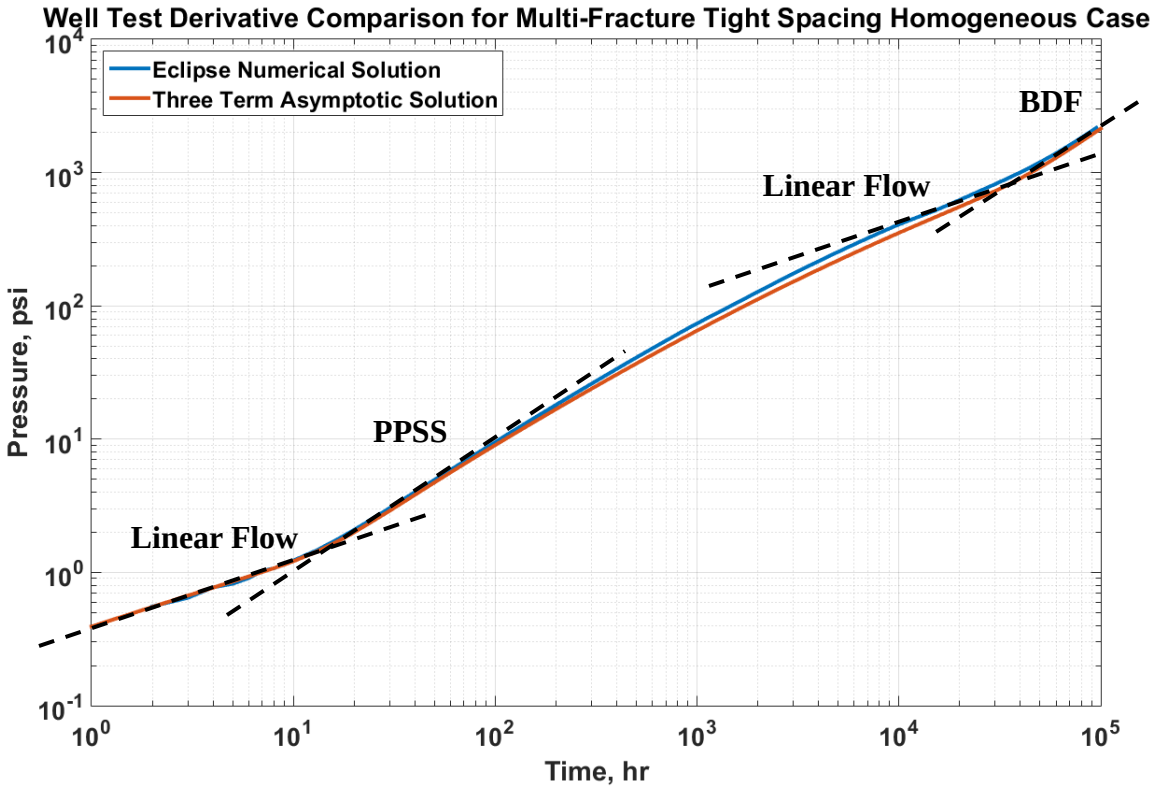

Fig.30 Well Test Derivative for Multiple Fractures Producing with Fixed Rate in Homogeneous Reservoir Case Calculated by Asymptotic Solution with Separation of Variables, Superposition, and Numerical Simulation

From the plot, we observe the well test derivative curves overlap during early time with a slope of one half which indicates fracture linear flow. This behavior accurately corresponds to our reservoir setup. Then the fracture interference occur, the curves start to deviate from the one half slope and follow a unit slope line which indicates a boundary dominated flow regime. However boundary dominated flow is not an appropriate interpretation in this situation. The cause of this unit slope is that when fractures interfere with each other, a portion of flow area is lost. Accordingly the well test derivative will follow through a transition period until it stabilizes into another flow

regime. The transition slope is usually very small and changes smoothly. However, when the flow area lost during fracture interference causes the original flow area to diminish by a magnitude, the transition period slope will become close to a unit slope. And it is proper to believe, if the loss reaches a higher magnitude, the slope will become even larger. Such flow behavior is generally observed in unconventional reservoirs and is identified as pseudo pseudo-steady state (PPSS) flow (Bo et al. 2011).

Soon after the pseudo pseudo-steady state flow, the asymptotic line start to deviate from the reference solution. This phenomenon is caused by the pressure diffusion propagating slower from fracture tip shown in Fig.31.

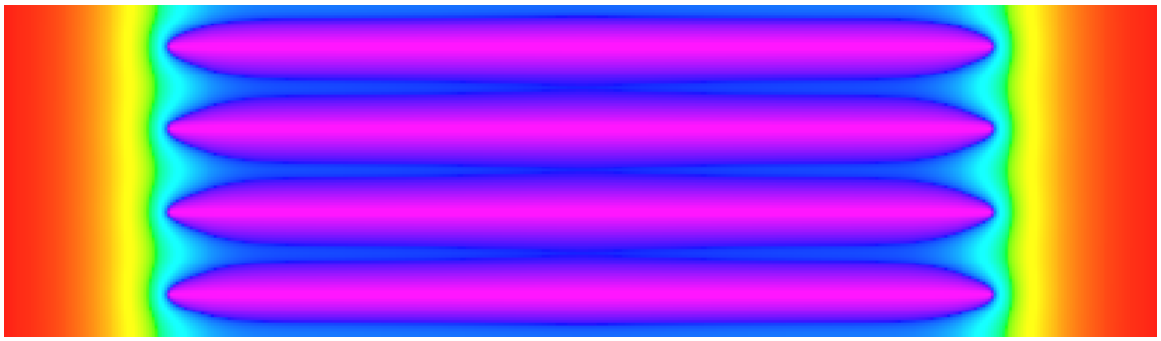

Fig.31 Pressure Map Generated by Eclipse for the Multiple Fracture with Tight Spacing in Homogeneous Reservoir Case Shows Sharps Edges at Fracture Tip

It is obvious from the above plot that the pressure contour leaves the pill box shape and tend to form sharp edges around the fracture tip. The difference in shapes between pressure contour and DTOF contour causes the well test derivative to diverge from the reference solution and incapable of capturing the second linear flow. Finally, the reservoir forms boundary dominated flow after the fractures felt the entire reservoir and

the curves overlap again. The flow behaviors indicated by the well test derivative aligns with the reservoir set up and more importantly we successfully model the PPSS flow regime.

The improvement we made here is that, by implementing reflection terms and applying separation of variables method, we can bring the flow regime closer to PPSS compared to the previous solution without reflection mechanism as illustrated in Fig.32.

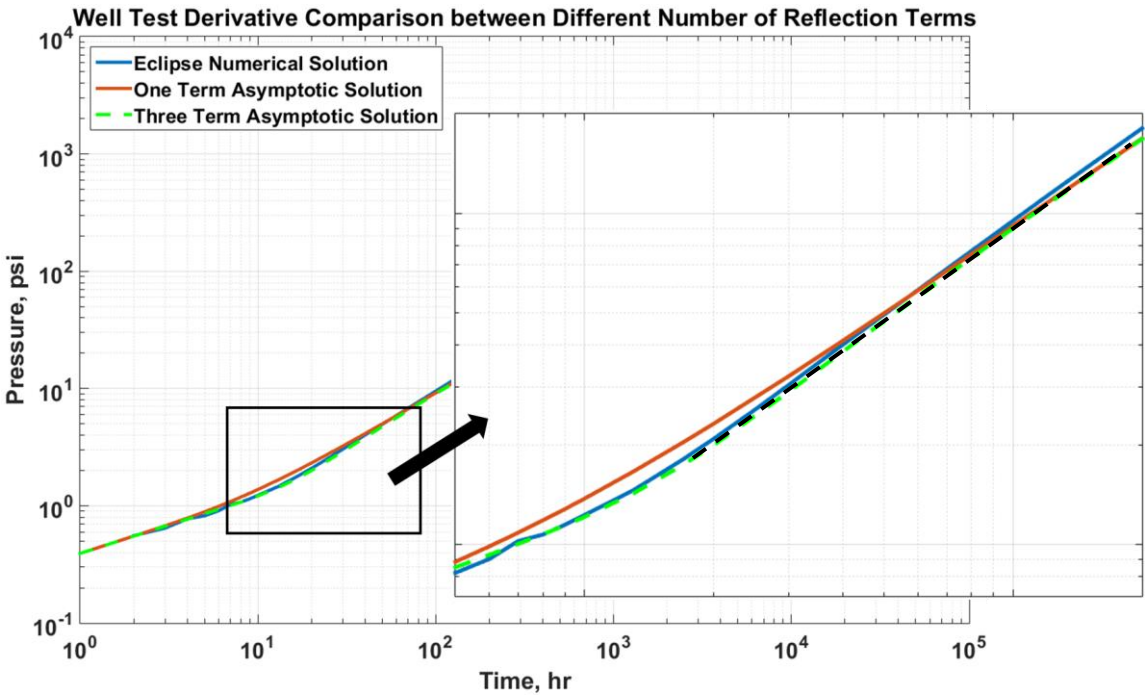

Fig.32 Three Terms Reflection Algorithm and Separation of Variables Models PPSS Flow Regime More Appropriately

We can observe the curve generated with no reflection terms (red curve) does not represent the PPSS flow regime at all.

3.3 Multiple Fracture with Tight Spacing Producing in Homogeneous Reservoir at Fixed Bottom Hole Pressure

Our methodology successfully models the PPSS in the multi-fracture fixed rate scenario. However, barely any wells nowadays are producing at a fixed rate, especially in unconventional reservoirs where production rate is usually unstable. Under such circumstances, in this section, we will investigate the fixed producing bottom hole pressure scenario.

We will use the exact same reservoir as the previous case and generate Rate Normalized Pressure derivative by Eq.(2.33). Considering the rate is constantly changing, if we still produce the diagnostic plot in physical time, all the flow regime vanishes as shown in Fig.33.

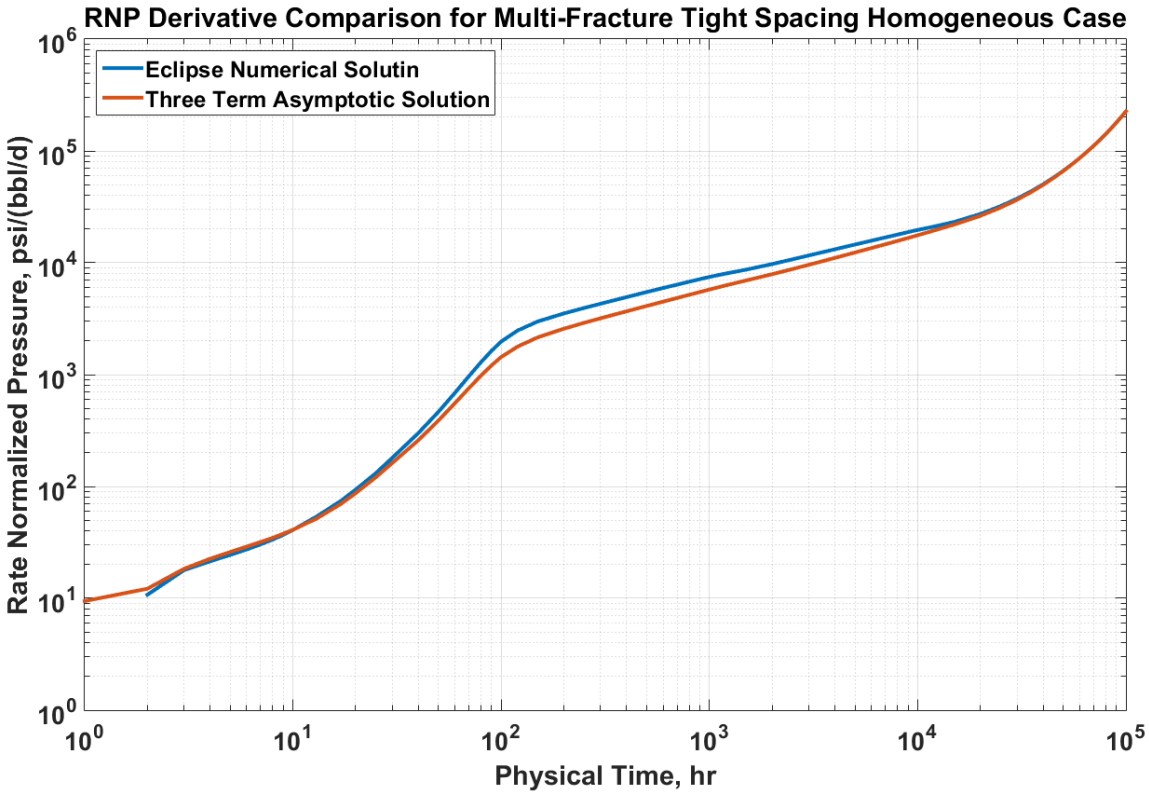

Fig.33 Rate Normalized Pressure Derivative for Multiple Fractures Producing with Fixed Bottom Hole Pressure in Homogeneous Reservoir Case Plotted in Physical Time Domain

Therefore in order to observe flow regimes, we will use material balance time as X axis. The material balance time is only completely valid and accurate in boundary dominated flow. However, it is a sufficiently accurate approximation during other flow regimes (Blasingame Thesis 1986). The result is illustrated in Fig.34.

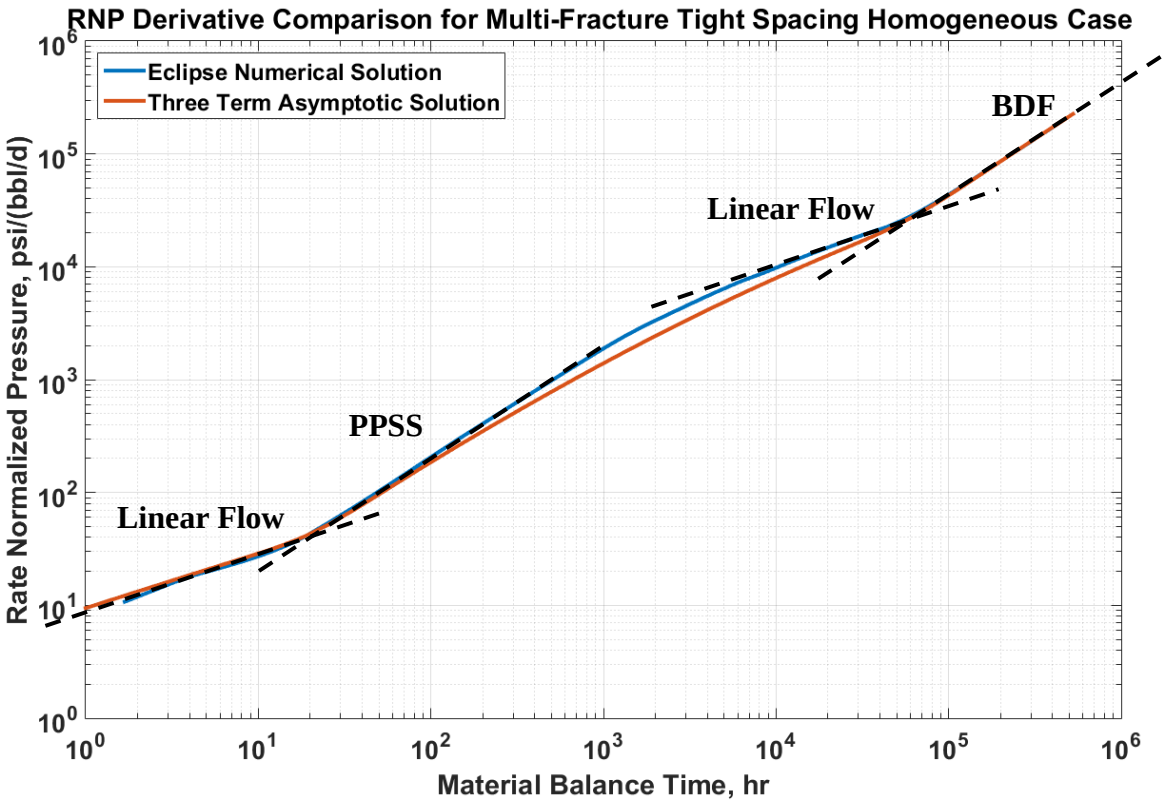

Fig.34 Rate Normalized Pressure Derivative for Multiple Fractures Producing with Fixed Bottom Hole Pressure in Homogeneous Reservoir Case Calculated by Asymptotic Solution with Separation of Variables and Numerical Simulation

The RNP derivative generally follows the same flow regimes as the well test derivative in the previous case. In both fixed rate and fixed bottom hole flowing pressure cases, we observe the PPSS flow regime generated by our solution is shorter compare to the one provided by the flow simulator. This is mainly because FMM assumes pressure diffusion from the fracture tip is as fast as the pressure diffusion along the fracture. It is also because of this same reason that our solution is incapable of capturing the second linear flow.

CHAPTER IV

HETEROGENEOUS MODEL EXTENSION

In the previous chapter, we already demonstrated the homogeneous cases results generated by three term asymptotic solution along with separation of variables. We successfully modeled the PPSS flow regime. In this chapter we will try to extend our methodology into the heterogeneous cases. We will first try to identify the stagnation line and develop separate directional DTOF variables. Then we will develop an appropriate way to represent the boundary conditions in presence of heterogeneity. Finally we will run the asymptotic algorithm for a smooth and a discontinuous heterogeneous case and show some results.

4.1 Identify Stagnation Line and Develop Separate Directional DTOF Variable

To incorporate the methodology we demonstrated in the previous chapter into heterogeneous systems, we generated two heterogeneous permeability fields. One of them is generated by sequential Gaussian simulation with 45 degree anisotropy and therefore is discontinuous. As a long reservoir, it is impossible to plot the entire permeability field while maintaining the correct aspect ratio. Therefore Fig.35 illustrates three sample sections.

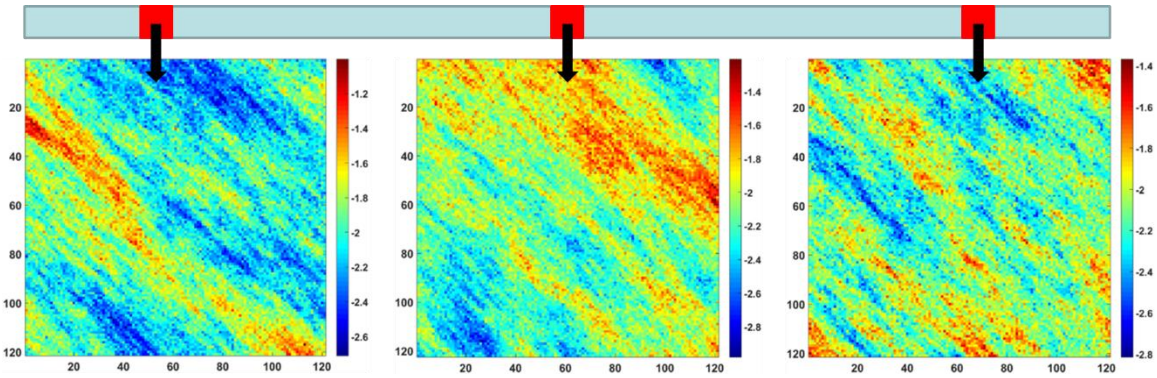

Fig.35 Discontinuous Permeability Generated by Sequential Gaussian Simulation

Another permeability field is a smooth model with less heterogeneity as demonstrated in Fig.36.

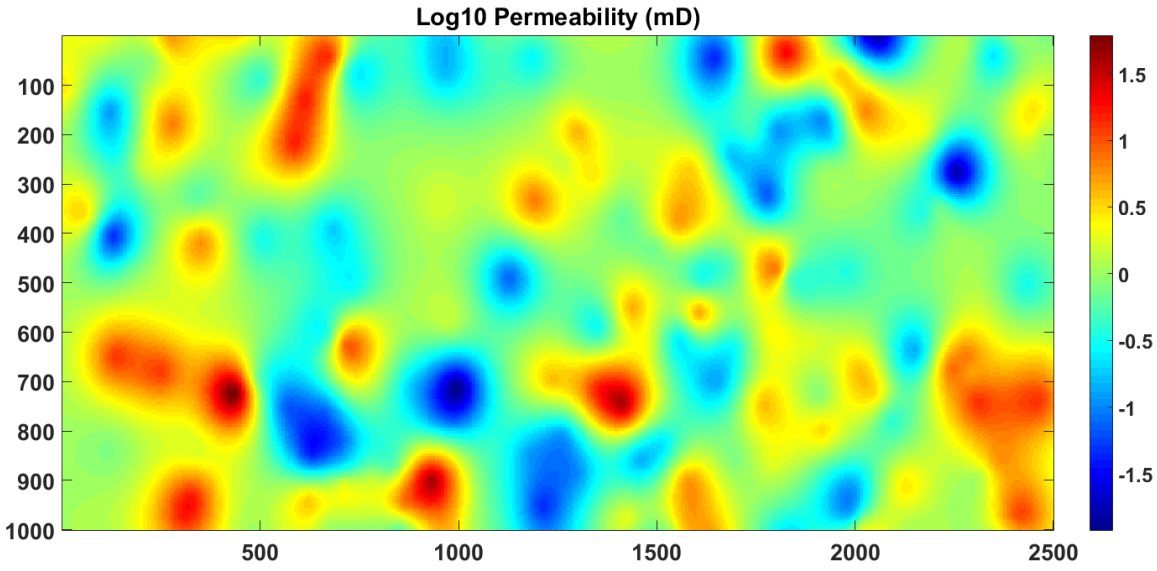

Fig.36 Smooth Heterogeneous Permeability Field Generated by Kriging

The first step to incorporate our methodology is to identify the stagnation lines which represents the boundary conditions. Our approach is to find the grid block with

local maximum DTOF value and a series of these grid blocks will constitute the stagnation line. The stagnation lines for the smooth model is plotted in black in Fig.37.

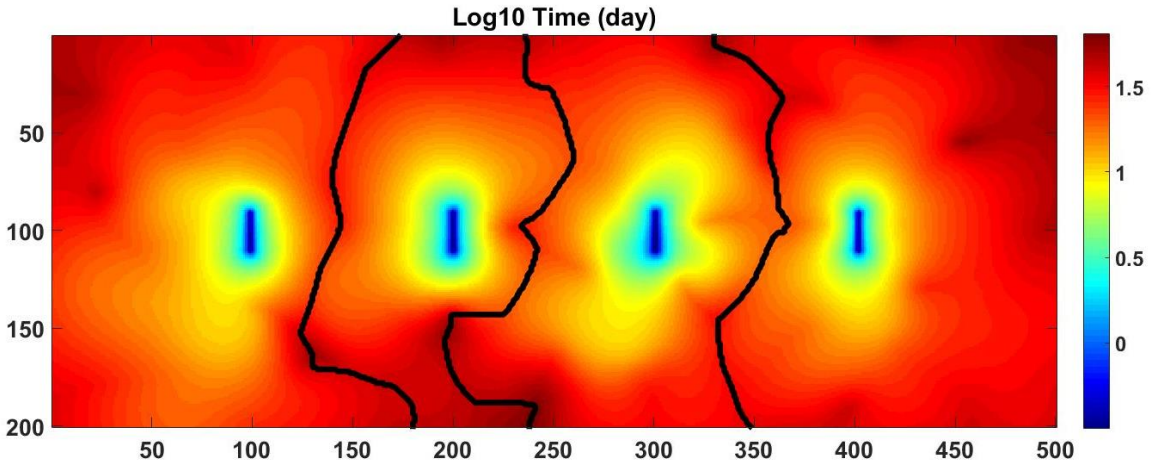

Fig.37 Diffusive Time of Flight of Four Fractures in Heterogeneous Reservoir with Stagnation Line Indicating Fracture Interference

These lines indicate fracture interference and with their help, we can separate each fracture and analyze their rate normalized pressure and drainage volume individually. In field cases, if we can capture drainage volume for fractures individually, we will be able to distribute the total production rate to each fracture accordingly since production rate is proportional to drainage volume. This helps fixing the current problem in the petroleum industry that we assume production is distributed uniformly among all fractures. Solving this problem will eventually increase reservoir forecast accuracy.

After finding the stagnation line, we need to decompose the total diffusive time of flight into X and Y directions. Determining τ_x and τ_y is not as easy in heterogeneous media since the simple geometric decomposition is no longer valid. In search for the

correct method of decomposition, we first plot the total DTOF long the stagnation line illustrated in Fig.38. We use the discontinuous heterogeneous case since it has a longer stagnation line and it is easier to observe certain behavior.

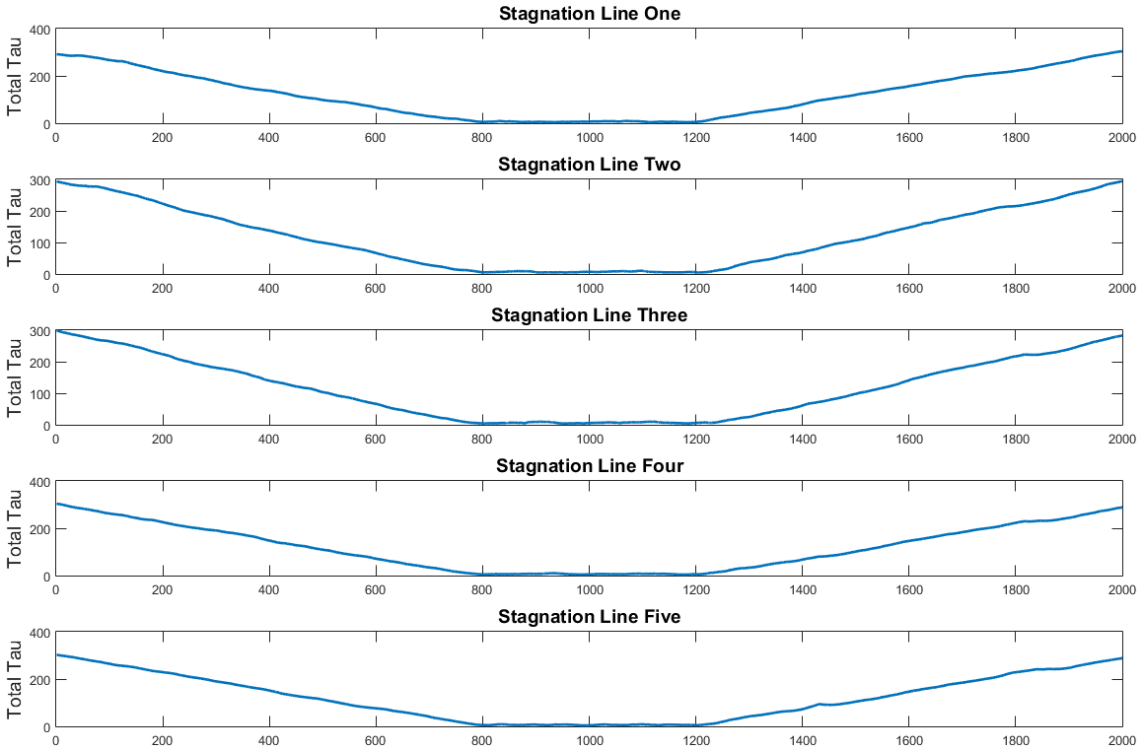

Fig.38 Total DTOF along Stagnation Lines Indicates Two Structures.

In the plot, we clearly observe that the DTOF values shows two structures. The region bounded by the fracture has fairly constant τ values while the region beyond fracture tips has linearly increasing τ values. We will use such behavior to construct our decomposition method for heterogeneous systems.

Recall that in homogeneous reservoir, after geometric decomposition, the τ_{dx} along boundary does not vary. Therefore, even though the τ_d along the stagnation line will slightly fluctuate due to the heterogeneity, with a correct decomposition method, the τ_{dx} value should stay fairly constant even with the presence of heterogeneity. Our decomposition method for heterogeneous system involves two FMM calculations as demonstrated in Fig.39.

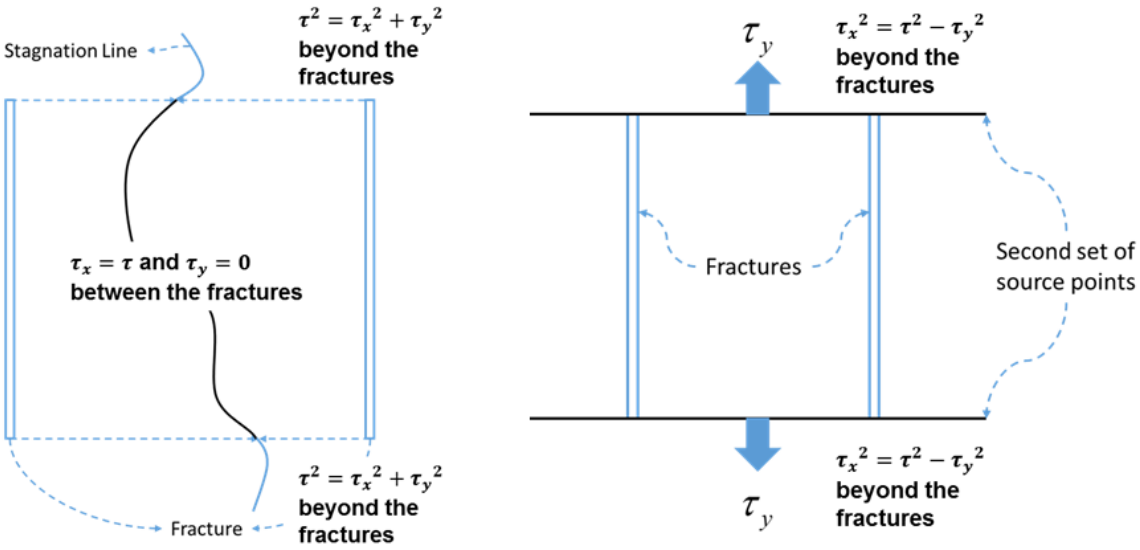

Fig.39 Using Two FMM Calculations to Produce Directional DTOF Variable

The first FMM calculation (left) is a usual one that propagates from the fractures. For the regions bounded by the fractures, $\tau = \tau_x$ and $\tau_y = 0$. For the regions beyond the fracture tips, $\tau^2 = \tau_x{}^2 + \tau_y{}^2$. For the second FMM calculation (right), we create another set of source points that connect the fracture tips and remove the original fracture source

points. We ignore the DTOF values for the regions bounded by the fracture. For the regions beyond the fracture tips, the DTOF is considered the τ_y.

We decompose the total DTOF for the smooth heterogeneous system using the two FMM calculation method and compare the result against geometric decomposition. The comparison is shown in Fig.40.

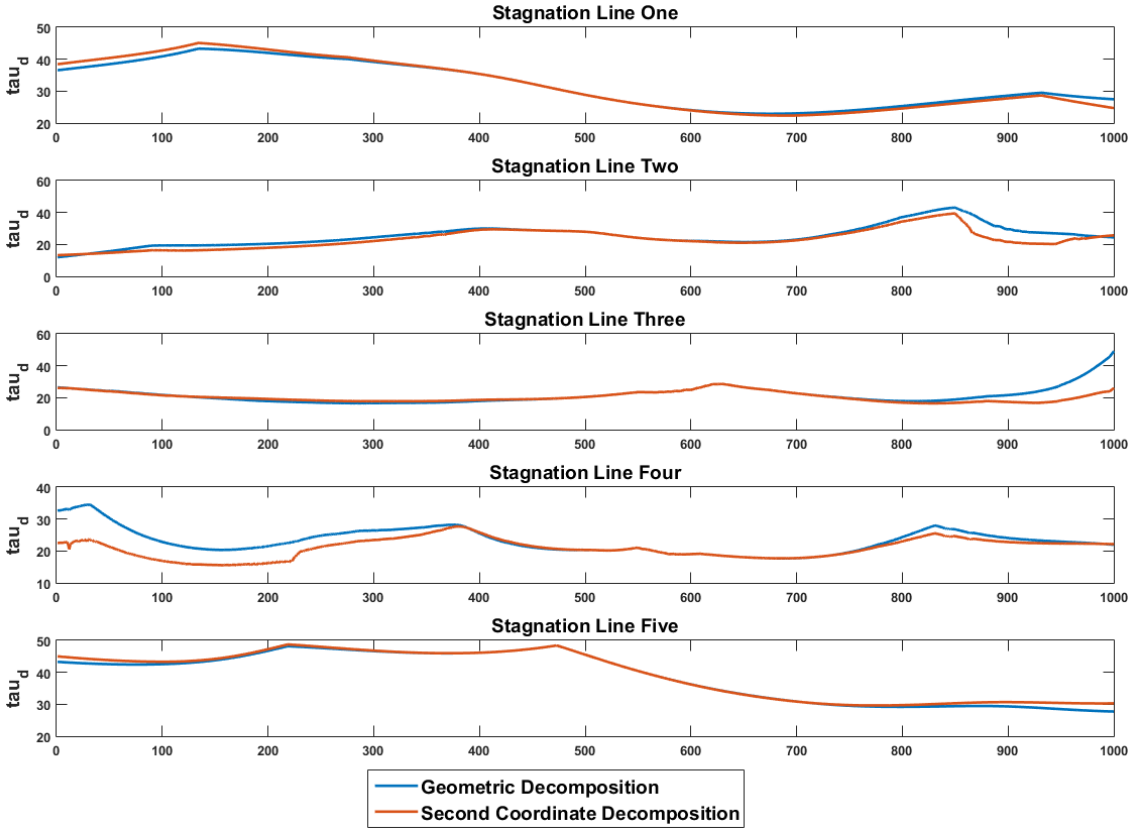

Fig.40 X Direction Diffusive Time of Flight along Stagnation Line Generated by Geometric Decomposition and Second Coordinate Decomposition in Smooth Heterogeneous System

In systems where the heterogeneity is smooth the two approaches of decomposition does not produce significantly distinct result. However, for systems with discontinuity, decomposing with a second set of source point to produce τ_y indicates clear advantage as shown in Fig.41.

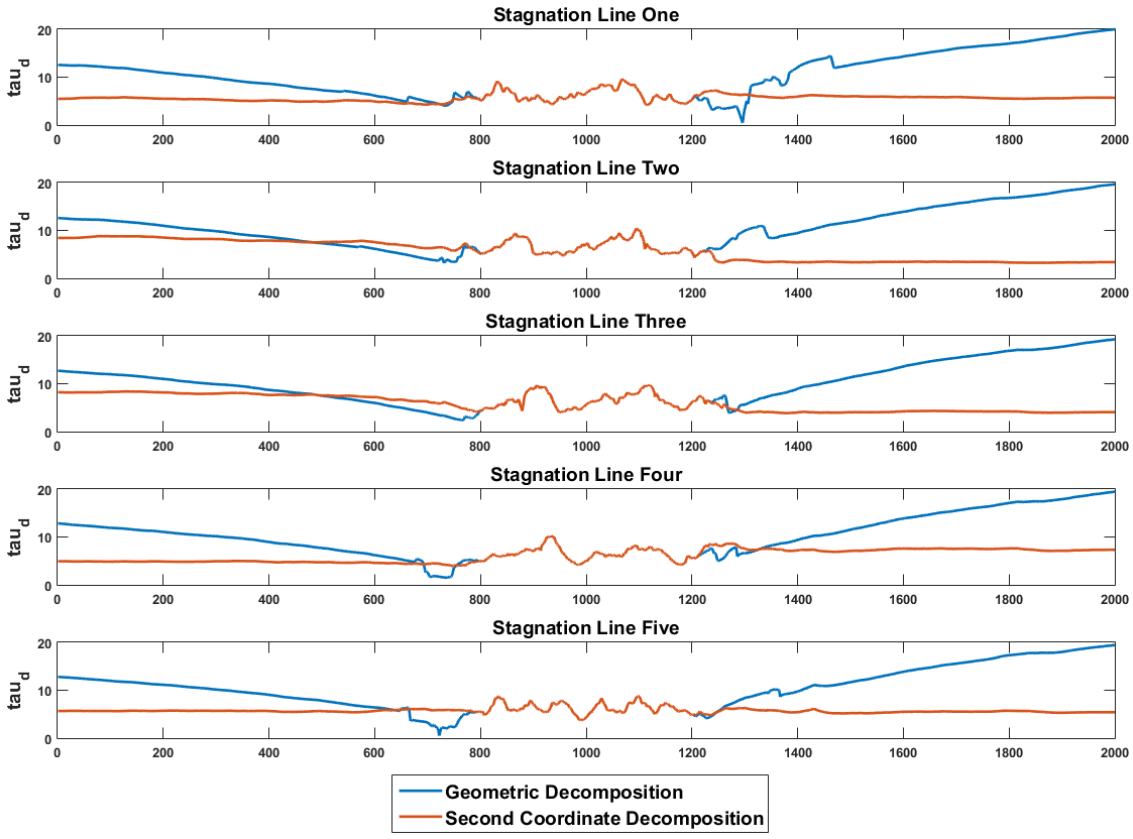

Fig.41 X Direction Diffusive Time of Flight along Stagnation Line Generated by Geometric Decomposition and Second Coordinate Decomposition in Discontinuous Heterogeneous System

Also, a directional DTOF contour map shown in Fig.42 indicates that we have successfully isolated the two structures observed in the stagnation line. Therefore, we

will decompose DTOF in heterogeneous media using a second set of source point to produce τ_y.

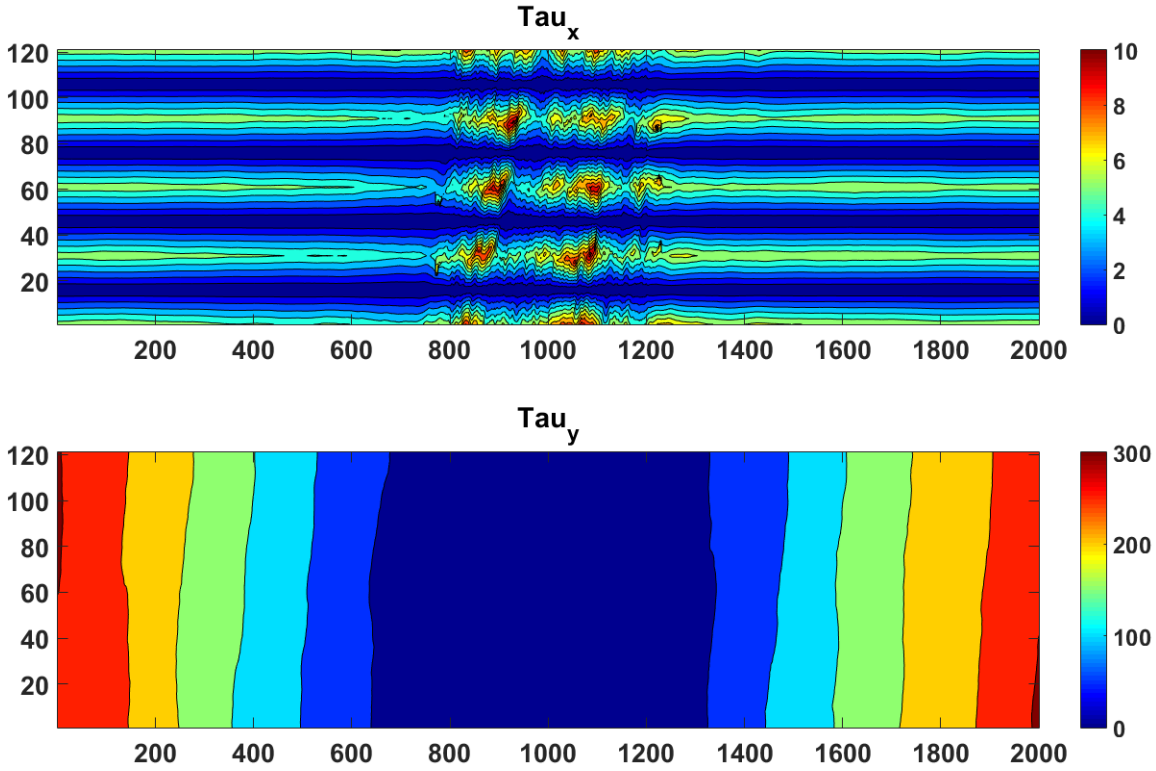

Fig.42 Decomposed Diffusive Time of Flight in X and Y Directions for Heterogeneous Case

After identifying the stagnation line and developing the decomposition method, we need to correctly represent the no flow boundary effect in heterogeneous media in order to model the reflection behavior. The first method we tried is called initial contact method where we use the initial interference point as the beginning of reflection observation. Such method causes significant amount of early drainage and thus is not appropriate.

The second method is to use the average DTOF along the section of the boundary parallel to the fracture. Fig.43 demonstrated how such τ_d value is obtained. We call this approach the average DTOF method.

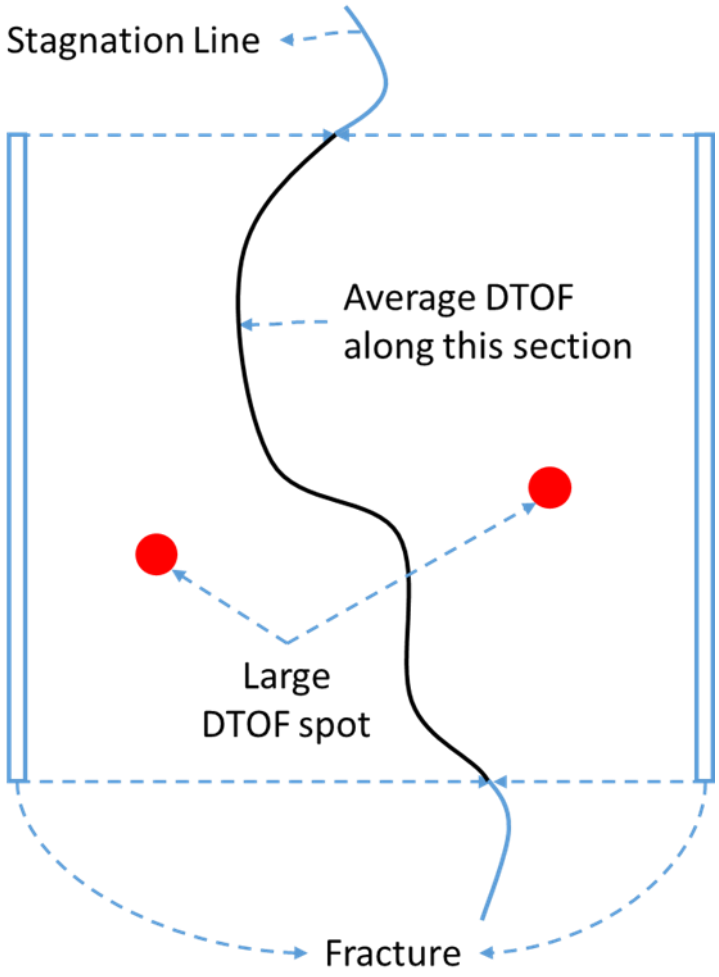

Fig.43 Average DTOF Method of Determining the DTOF that Indicates Reflection Observation

In heterogeneous media, it is highly possible to encounter some region with extremely low permeability and thus high τ value. Such high τ value can potentially

cause the term $2\tau_d - \tau$ to become negative, causing the region to drain before it should. To counter this problem we eliminate the reflection terms in these cells with extremely high τ value to prevent their early drainage. The threshold to determine whether a τ value is high enough to eliminate the reflection terms is by the τ_d acquired using average DTOF method. A drainage volume comparison map is plotted in Fig.44.

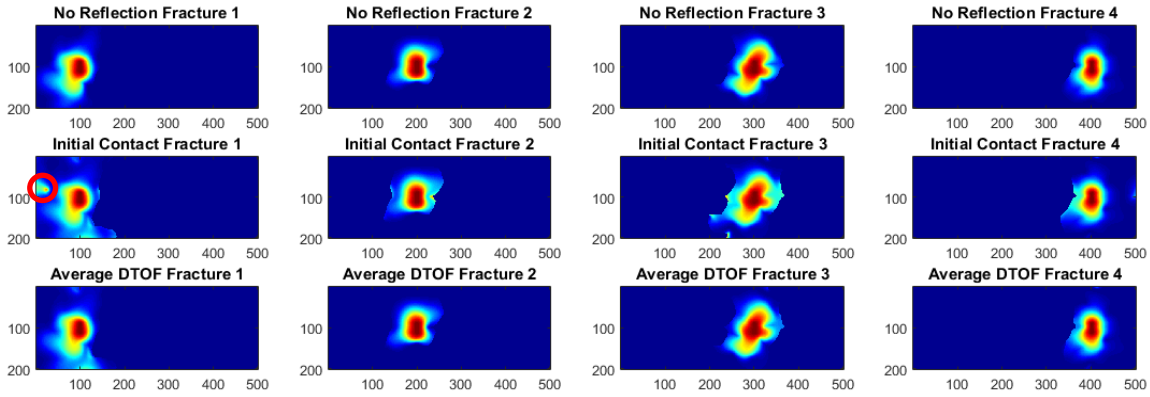

Fig.44 Individual Fracture Drainage Volume Map Comparison between Different Asymptotic Solution Methods at a Picked Time Point

As we can see, the average DTOF method prevents early drainage behavior as indicated by the red circle.

4.2 Multiple Fractures Producing at Fixed Pressure in Smooth Heterogeneous Reservoir

In the last section, we identified stagnation line and developed the decomposition method for heterogeneous systems. We also determined that using the average DTOF

method is the most appropriate way to represent boundaries in heterogeneous reservoirs. Therefore in this section, we will test the smooth heterogeneous case and compare the result from our methodology to the one from numerical simulation.

Let us first look at the well drainage volume and RNP derivative illustrated below.

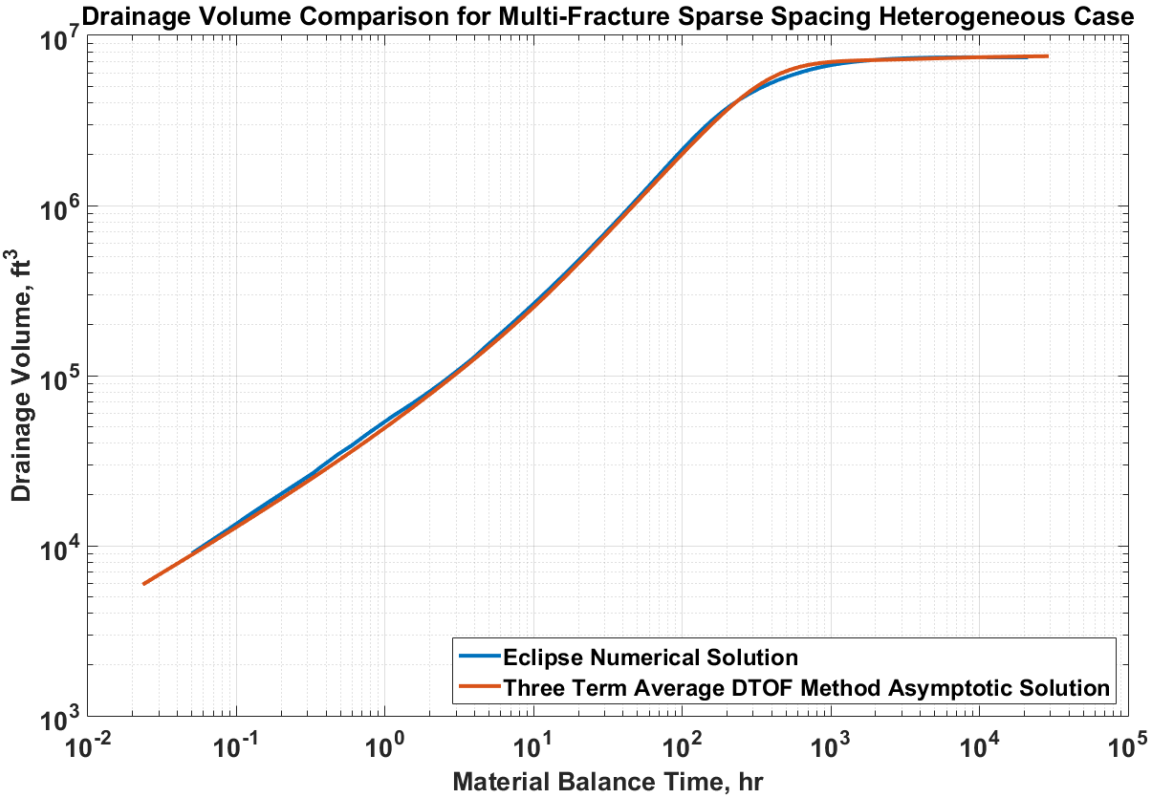

Fig.45 Total Well Drainage Volume Comparison between Average DTOF Method and Eclipse Numerical Simulation for Heterogeneous Case

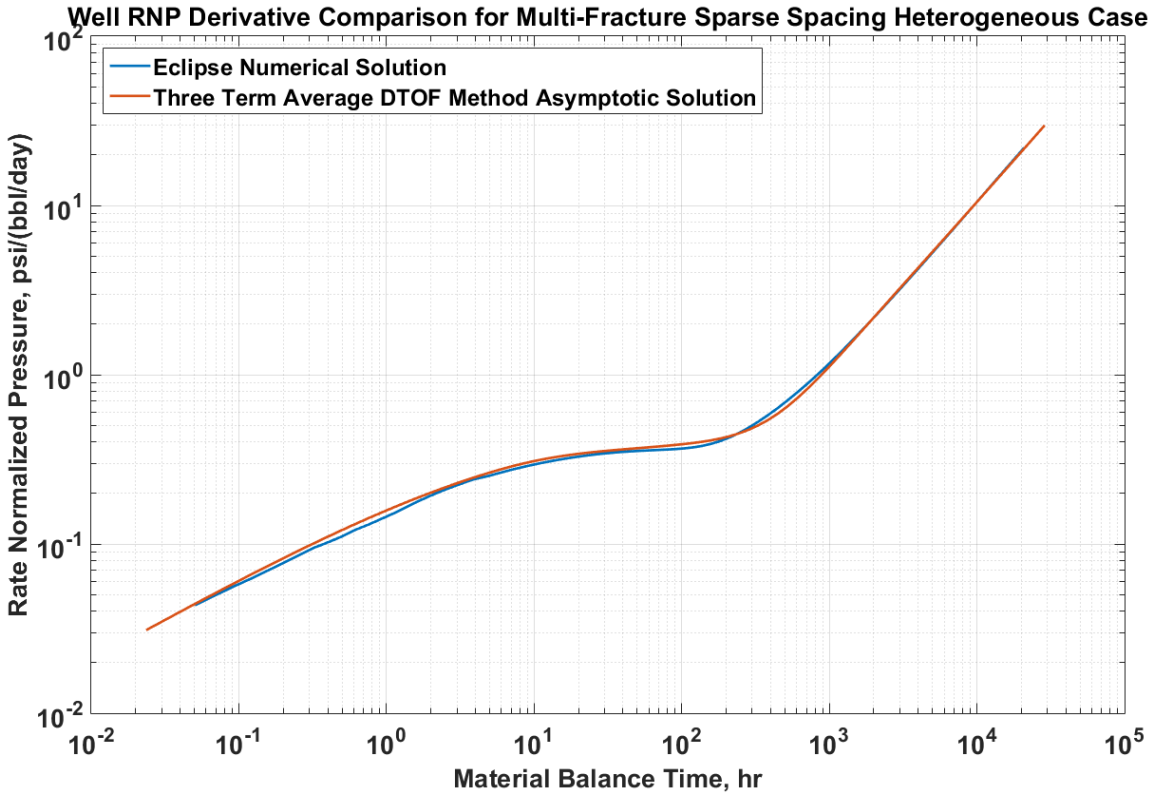

Fig.46 Total Well Rate Normalized Pressure Derivative Comparison between Average DTOF Method and Eclipse Numerical Simulation for Heterogeneous Case

We observe that for well analysis, the drainage volume and RNP derivative curves generally overlaps, indicating the algorithm has captured the correct reservoir features.

Since we have the coordinates of the stagnation line, we can also conduct individual fracture analysis. The drainage volume and RNP derivative for individual fracture is plotted in Fig.47 and Fig.48.

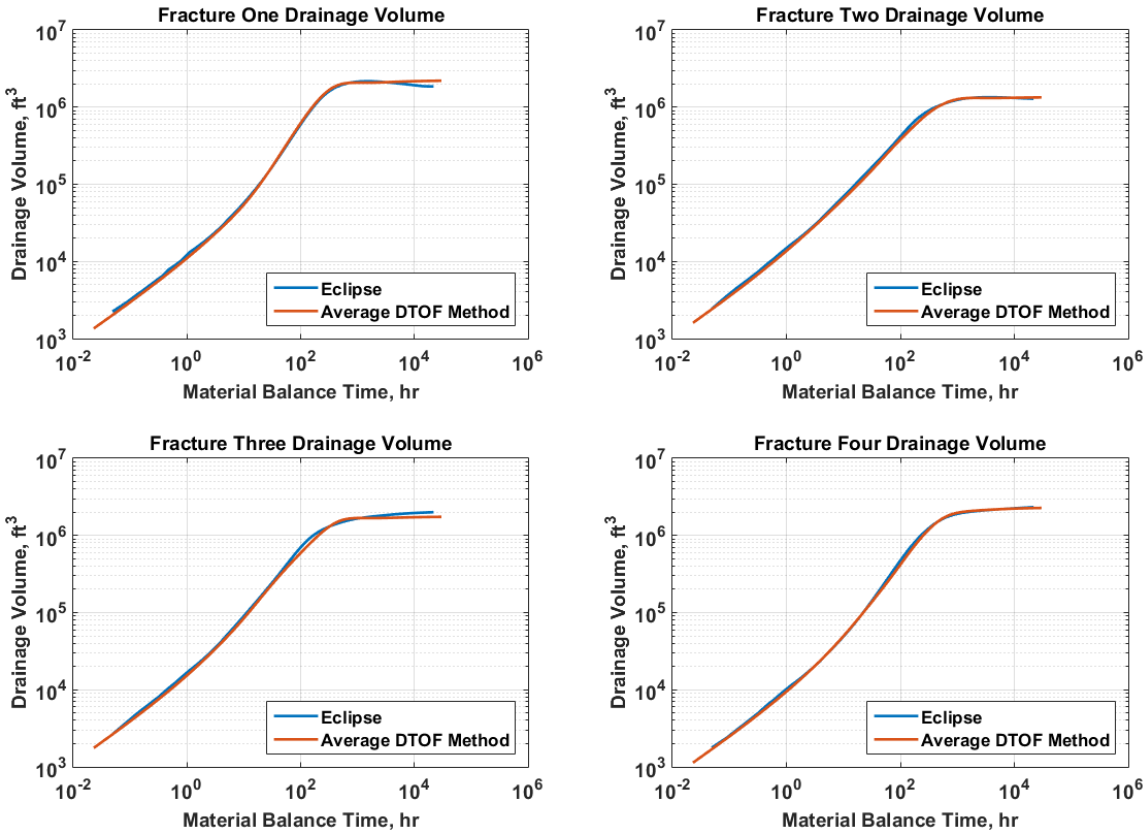

Fig.47 Individual Fracture Drainage Volume Derivative Comparison between Average DTOF Method and Eclipse Numerical Simulation for Heterogeneous Case

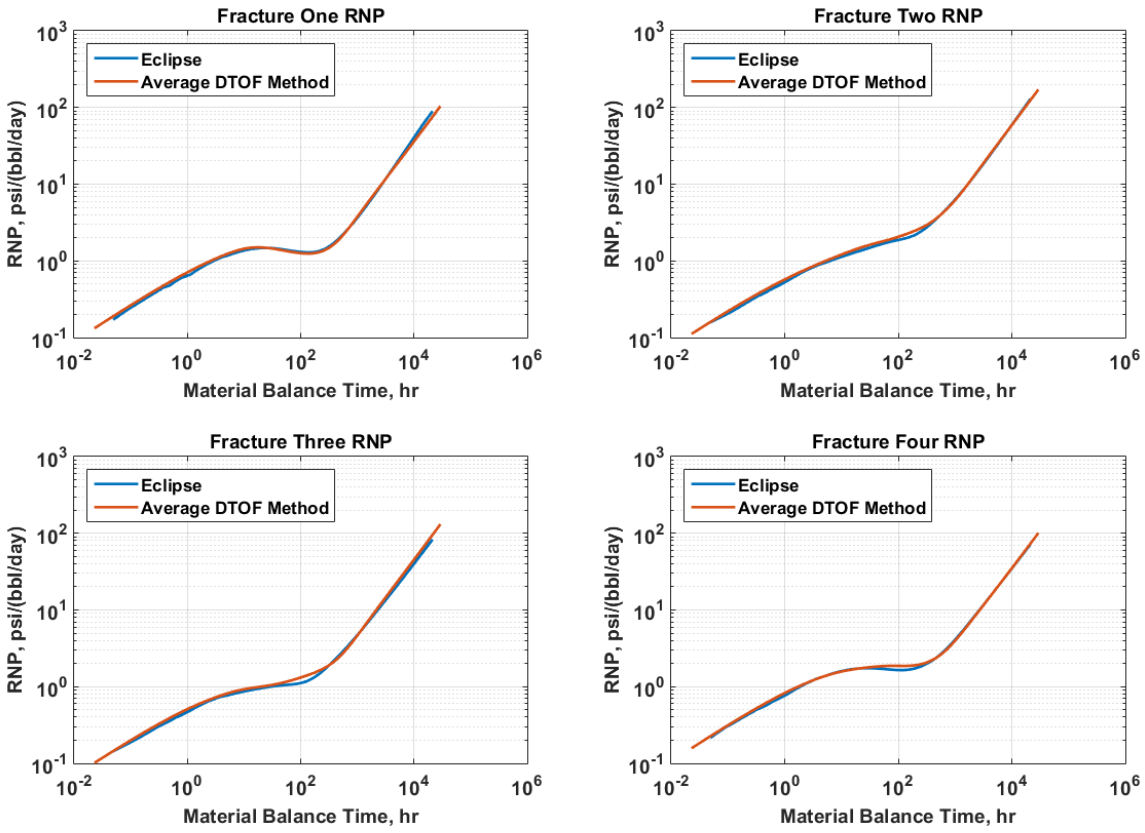

Fig.48 Individual Fracture Rate Normalized Pressure Comparison between Average DTOF Method and Eclipse Numerical Simulation for Heterogeneous Case

The result for individual fracture shows same behavior as the well analysis. The above plots indicates that our methodology is correctly implemented in heterogeneous systems.

4.3 Multiple Fracture with Tight Spacing Producing in Heterogeneous Reservoir at Fixed Bottom Hole Pressure

The main goal is to model pseudo pseudo-steady state flow in heterogeneous reservoir since it is signature behavior of unconventional reservoir. Therefore the last case we will analyze is fractures with tight spacing producing in heterogeneous media.

In order to be more realistic, we use the discontinuous permeability field generated by sequential Gaussian simulation with a 45 degree of anisotropy.

We use the same algorithm as the last section to calculate the total well RNP. The result is illustrated in Fig.49.

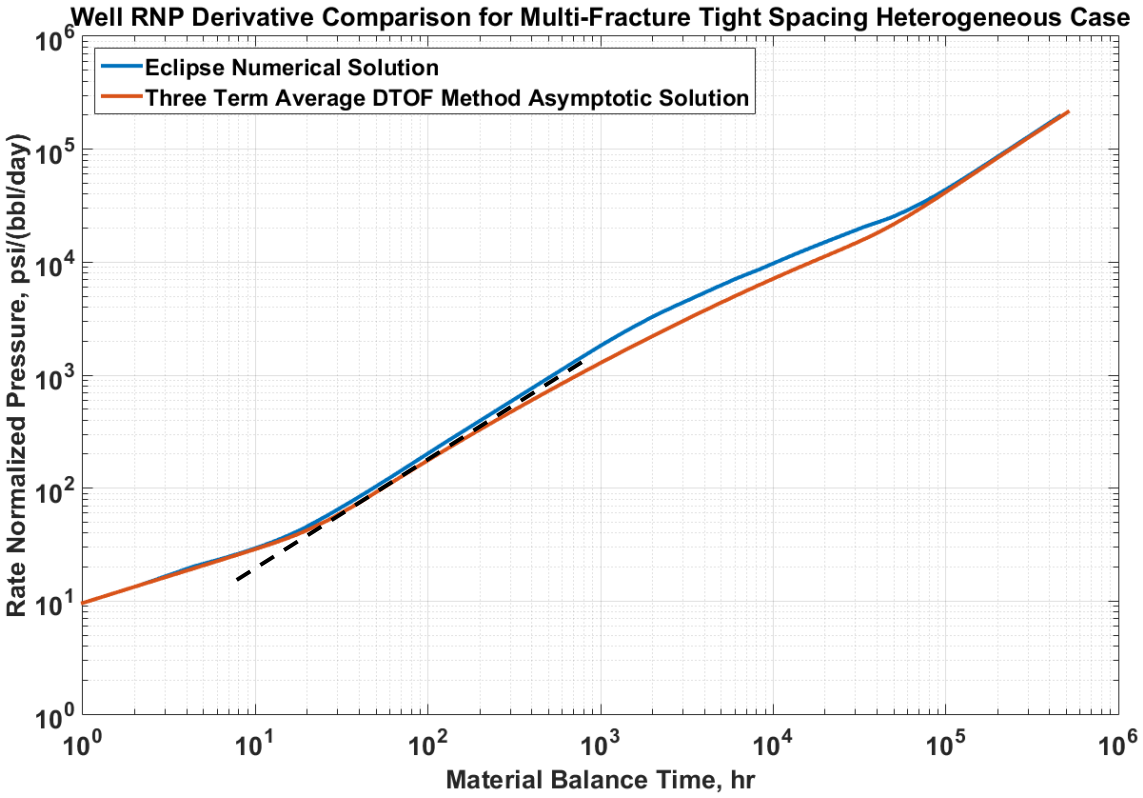

Fig.49 Total Well RNP for Tight Spacing Fractures Producing in Heterogeneous Reservoir Indicating PPSS Flow Regime

We observe that even with error caused by our assumption that the pressure contour is the same as DTOF contour, the model still returns a positive unit slope for RNP derivative that indicates PPSS. However, the time span for PPSS generated with our model is shorter than the reference solution.

We also calculated RNP for individual fractures. The results are illustrated in Fig.50.

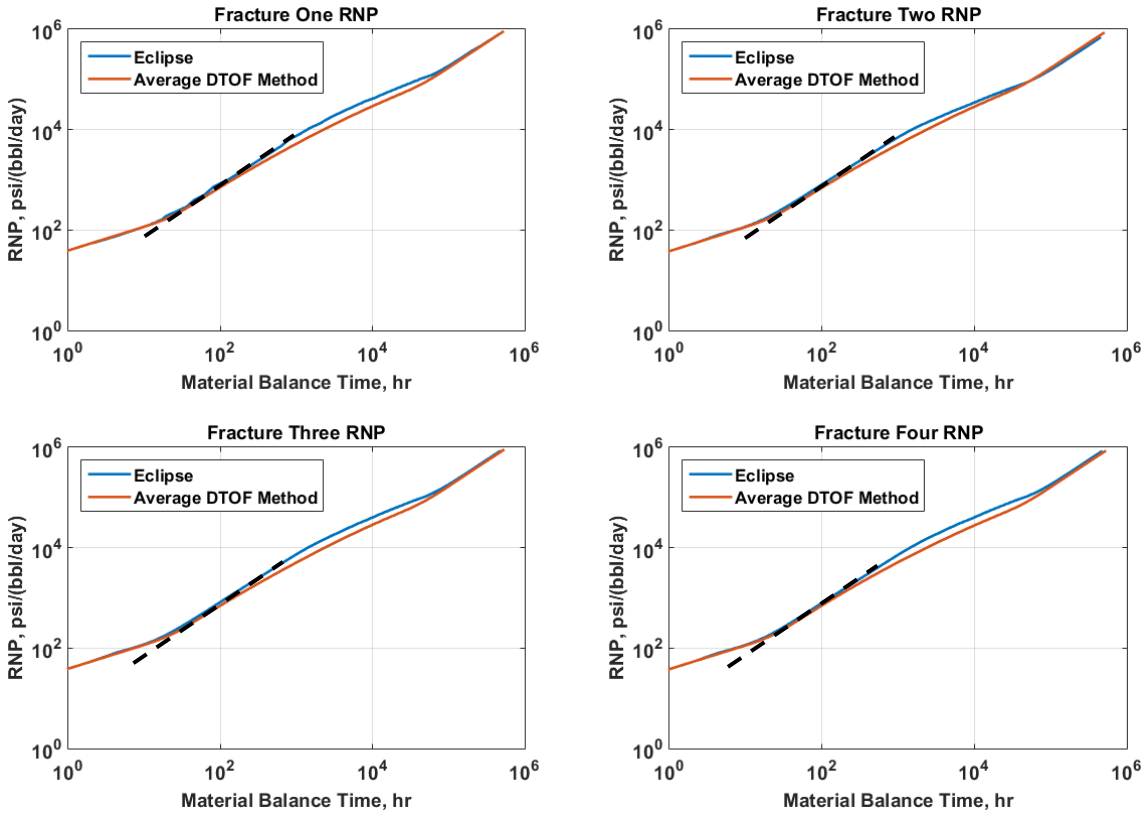

Fig.50 Individual Fracture RNP for Tight Spacing Fractures Producing in Heterogeneous Reservoir Indicating PPSS Flow Regime

We see the same behavior on individual fracture RNP as the well RNP. Each of these fractures experiences PPSS after their fracture linear flow is finished.

The last step is always to check the improvement with our methodology compared to previous one. The comparison is plotted in Fig.51.

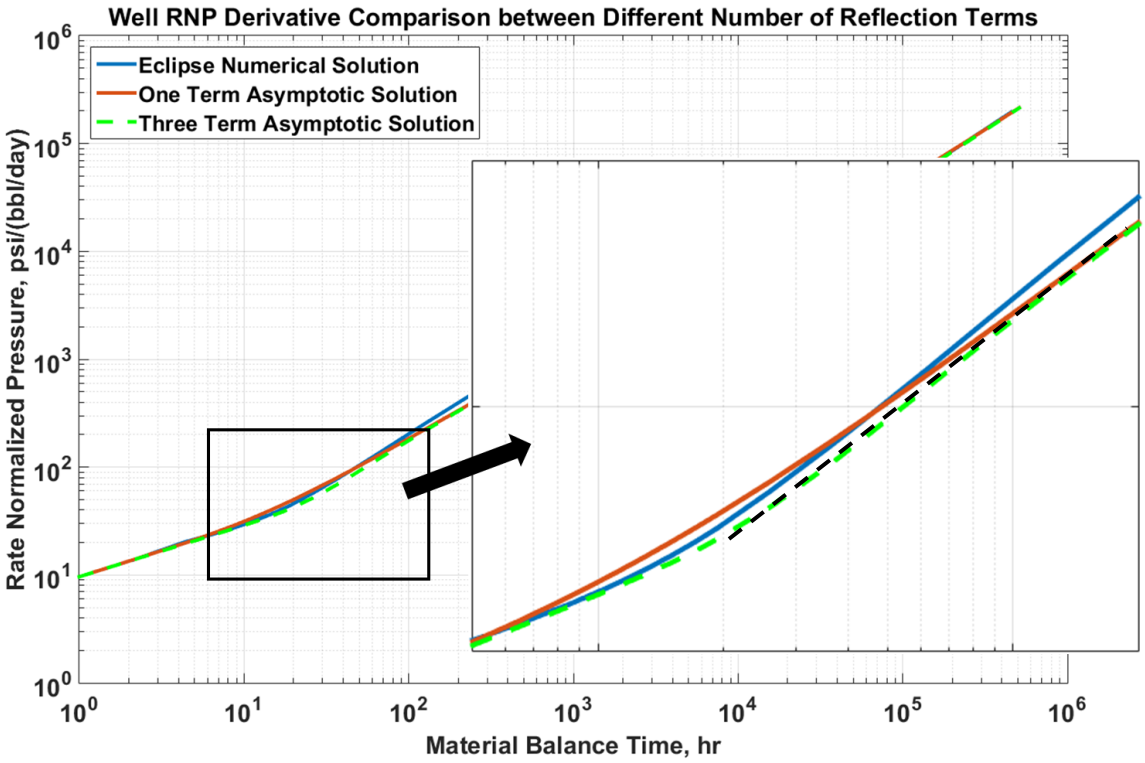

Fig.51 Total Well RNP Calculated with and without Reflection Mechanism Comparison

In the zoomed in view, we clearly notice the new method captures the PPSS flow regime while the old method completely disregards such behavior.

On the other hand, if we plot 1/RNP versus physical time, we obtained a decline curve behavior illustrated in Fig.52.

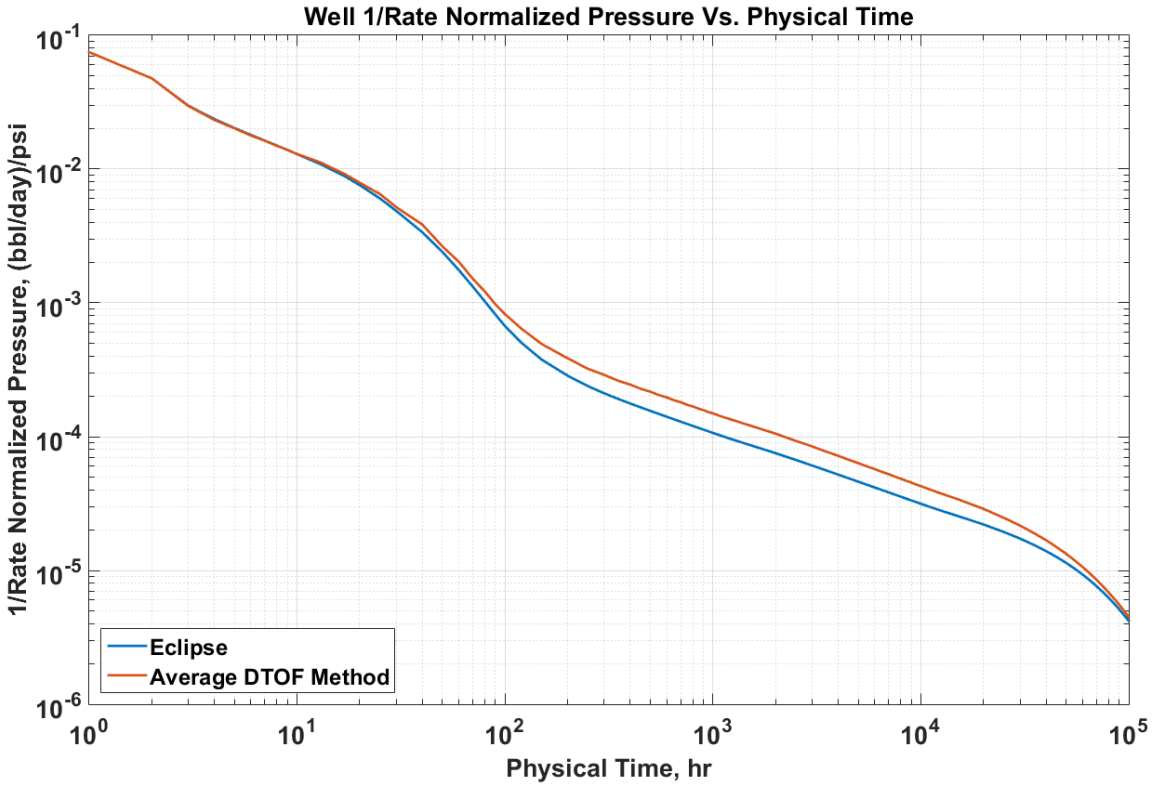

Fig.52 1/RNP Plotted Against Physical Time Shows Decline Curve Behavior

The error during middle time (around 1500 hours) is 40%. However this does not cause a significant error when estimating production rate and EUR since the 1/RNP is already very low at this time range.

CHAPTER V

CONCLUSION & RECOMMENDED FUTURE WORK

5.1 Summary and Conclusions

This thesis introduces a new approach, the separation of variables method, to model reflection mechanism of pressure diffusion in heterogeneous reservoir. The main target application is unconventional reservoirs where most wells drilled are horizontal wells with multiple hydraulic fractures. As these fractures interfere with each other and create virtual boundaries, the significant loss of flow area causes the pressure derivative or rate normalized pressure derivative to form a unit slope even though the reservoir has not achieved boundary dominated flow. We call such flow regime as Pseudo Pseudo-steady state flow. This new approach successfully models such flow regime analytically without using the flow simulator. By achieving so, we hope to calibrate and forecast the reservoir faster with the analytical solution and also to capture the correct feature of the reservoir. The main conclusions are summarized as follow.

- The separation of variable algorithm which is inspired by integrating in Cartesian coordinate system for a cycle area can be applied to vertical well scenarios. By doing so we can achieve a better pressure solution for channel reservoir since we can model boundary conditions in different directions separately.
- To model the boundary conditions, we need to incorporate additional terms in our mathematical formulation to capture the pressure diffusion reflecting from

the boundary. By analysis, we determined that two reflection terms and one outgoing term (three term formulation) is enough to model the reflection mechanism. Adding extra terms beyond three only increases the calculation load while not returning more accurate results.

- To model the boundary conditions in heterogeneous reservoirs, we need to first determine the stagnation line created by adjacent fractures interfering with each other. The stagnation line is pinpointed by searching the local maximum DTOF. With the stagnation line, we can analyze fractures individually.
- The boundary diffusive time of flight value determined by average DTOF method as demonstrated by Fig.43 minimized the error when modeling reflection in heterogeneous systems. Using the initial contact point method causes early drainage at locations with low permeability.
- We need to filter out regions with high diffusive time of flight value caused by low permeability and erase the reflection from those regions in order to minimize error in drainage volume calculation.
- To decompose the total diffusive time of flight into X and Y directions, we can use the geometric method for homogeneous cases. For heterogeneous cases, we need to employ the approach illustrated by Fig.42. A correct decomposition method should return a rather constant boundary diffusive time of flight along the stagnation line.
- To model fracture cases, if the fracture length is relatively small regarding to the whole reservoir, our method can still return correct pressure behavior comparing

against simulation result. However, when analyzing long fracture tight spacing cases, the mismatch is obvious. This is caused by pressure contour becoming inconsistent with our diffusive time of flight contour which is contradictory with our initial assumption.

- Regardless to the discrepancies observed in long fracture tight spacing cases, our method still models the pseudo pseudo-steady state flow regime, however with a shorter time span compared to numerical simulation results.

5.2 Recommendations

Regarding the discrepancies found in long fracture tight spacing cases, we confirm that the pressure contour will not be align with the diffusive time of flight contour in fracture cases as time goes on. Therefore, the future work should focus on investigating the cause of such misalignment.

- Simulate cases with different fracture length in the same reservoir. Observe how the pressure behavior changes as fracture length increase and try to obtain a correlation between fracture length and the misalignment between pressure contour and diffusive time of flight contour.
- Extend the separation of variables method to the entire reservoir instead of only modeling pressure behavior at the well/fracture. By doing so, we can obtain an error map which is extremely beneficial for improving our algorithm.

- Attempt to model different pressure diffusion speed across the fracture with asymptotic solution so that we can minimize the mismatch observed in fracture cases.
- Try to calculate shape factors that correct the diffusive time of flight contour shape into flow simulator pressure contour shape.

REFERENCES

Bourdet, D., Whittle, T., Douglas, A., & Pirard, Y. (1983). A New Set of Type Curves Simplifies Well Test Analysis. World Oil, 95-106

Blasingame, T.A. (1986). Variable-Rate Analysis: Transient and Pseudo-steady State Methods of Interpretation and Application (Master's Thesis). Texas A&M University.

Cipolla, C. L., Lolon, E., Erdle, J., & Tathed, V. S. (2009, January 1). Modeling Well Performance in Shale-Gas Reservoirs. Society of Petroleum Engineers. SPE/EAGE Reservoir Characterization and Simulation Conference. Abu Dhabi, UAE. doi:10.2118/125532-MS

Cullick, A. S., Carrillo, M., Clayton, C., & Ceyhan, I. (2014, April 1). Well-spacing Study to Develop Stacked Tight Oil Pay in Midland Basin. Society of Petroleum Engineers. SPE Unconventional Resources Conference. Woodlands, Texas, USA. doi:10.2118/168992-MS

Datta-Gupta, A. and King, M.J. 2007. Streamline Simulation: Theory and Practice. Textbook Series #11. Richardson, TX: ISBN 978-1-55563-111-6.

Datta-Gupta, A., Xie, J., Gupta, N., King, M. J., & Lee, W. J. (2011, July 1). Radius of Investigation and its Generalization to Unconventional Reservoirs. *Journal of Petroleum Technology*, 63(7), 52-55. doi:10.2118/0711-0052-JPT

Dinh, A. V., Ajisafe, F. O., Tudor, J., Wisebaker, A., & Eke, C. (2015, March 1). A Reservoir Characterization and Simulation Modeling Study of the Third Bone Spring, Permian Basin. Society of Petroleum Engineers. SPE Production and

Operations Symposium. Oklahoma City, Oklahoma, USA. doi:10.2118/173600-MS

Fetkovich, M. J. (1980, June 1). Decline Curve Analysis Using Type Curves. Society of Petroleum Engineers. doi:10.2118/4629-PA

Friedrich, M., & Milliken, M. (2013, August 12). Determining the Contributing Reservoir Volume from Hydraulically Fractured Horizontal Wells in the Wolfcamp Formation in the Midland Basin. Unconventional Resources Technology Conference. Denver, Colorado, USA. URTEC-1582170-MS

Gringarten, A. C., Al-Lamki, A., Daungkaew, S., Mott, R., & Whittle, T. M. (2000, January 1). Well Test Analysis in Gas-Condensate Reservoirs. Society of Petroleum Engineers. SPE Annual Technical Conference and Exhibition. Dallas, Texas, USA. doi:10.2118/62920-MS

Hawkins, M. F. (1956). A Note on the Skin Effect. *Trans*. AIME, 207, 356-357

Jackson, J. D. (1998). *Classical Electrodynamics (3rd ed.)* New York: John Wiley & Sons.

King, M. J., Wang, Z., & Datta-Gupta, A. (2016, May 30). Asymptotic Solutions of the Diffusivity Equation and Their Applications. Society of Petroleum Engineers. SPE Europec. Vienna, Austria. doi:10.2118/180149-MS

Kulkarni, K. N., Datta-Gupta, A., & Vasco, D. W. (2000, January 1). A Streamline Approach for Integrating Transient Pressure Data into High Resolution Reservoir Models. Society of Petroleum Engineers. SPE European Petroleum Conference. Paris, France. doi:10.2118/65120-MS

Lee, W.J. 1982. *Well Testing*. Richardson, TX: Society of Petroleum Engineers.

Matthews, C. S., Brons, F., & Hazebroek, P. (1954, January 1). A Method for Determination of Average Pressure in a Bounded Reservoir. Society of Petroleum Engineers.

Muskat, M. (1949). *Physical Principles of Oil Field Production*. New York: McGraw-Hill Book Co.

Rincones, M. D., Lee, W. J., & Rutledge, J. M. (2015, November 9). Production Forecasting for Shale Oil: Workflow. Society of Petroleum Engineers. SPE Asia Pacific Unconventional Resources Conference and Exhibition. Brisbane, Australia. doi:10.2118/177018-MS

Satman, A., Eggenschwiler, M., & Ramey, H. J. (1980, January 1). Interpretation of Injection Well Pressure Transient Data in Thermal Oil Recovery. Society of Petroleum Engineers. SPE California Regional Meeting. Los Angeles, California, USA. doi:10.2118/8908-MS

Sethian, J. A. 1996. A Fast Marching Level Set Method for Monotonically Advancing Fronts. Proceedings of the National Academy of Science 93: 1591-1595.

Song, B., & Ehlig-Economides, C. A. (2011, January 1). Rate-Normalized Pressure Analysis for Determination of Shale Gas Well Performance. Society of Petroleum Engineers. North American Unconventional Gas Conference and Exhibition. Woodlands, Texas, USA. doi:10.2118/144031-MS

U.S. Energy Information Administration (2016, August). Annual Energy Outlook 2016. DOE/EIA-0383(2016).

Valko, P. P., & Lee, W. J. (2010, January 1). A Better Way To Forecast Production From Unconventional Gas Wells. Society of Petroleum Engineers. SPE Annual Technical Conference and Exhibition. Florence, Italy. doi:10.2118/134231-MS

Vasco, D. W., Keers, and H., Karasaki, K. 2000. Estimation of Reservoir Properties Using Transient Pressure Data: An Asymptotic Approach. Water Resour. Res. 36: 3447-3465.

Virieux, J., Flores-Luna, C., and Gibert, D. 1994. Asymtotic Theory for Diffusive Electromagnetic Imaging. Geophysical Journal International 119: 857-868.

Xie, J., Yang, C., Gupta, N., King, M. J., & Datta-Gupta, A. (2015, April 1). Integration of Shale-Gas-Production Data and Microseismic for Fracture and Reservoir Properties With the Fast Marching Method. *SPE Journal*, 2(20), 347-359. doi:10.2118/161357-PA

Xie, J., Yang, C., Gupta, N., King, M. J., & Datta-Gupta, A. (2015, August 1). Depth of Investigation and Depletion in Unconventional Reservoirs With Fast-Marching Methods. Society of Petroleum Engineers. SPE Europec. Copenhagen, Denmark. doi:10.2118/154532-PA

Yang, C., Sharma, V. K., Datta-Gupta, A., & King, M. J. (2015, July 20). A Novel Approach for Production Transient Analysis of Shale Gas/Oil Reservoirs. Unconventional Resources Technology Conference. doi:10.15530/URTEC-2015-2176280